Decoding Passenger's Brain Signals to Detect and Analyze Emergency Road Events

by

Junwen Fu

A thesis submitted to the Faculty of Graduate and Postdoctoral Affairs in partial fulfillment of the requirements for the degree of

Master of Applied Science

in

Electrical and Computer Engineering with Specialization in Data Science

Carleton University
Ottawa, Ontario

Abstract

With an increasing number of vehicles with automated functions on the road, road safety is still one of the biggest concerns for autonomous vehicles. Multiple crash reporting for vehicles shows the limitations of sensors and algorithms on vehicles equipped with Advanced Driver Assistance Systems (ADAS) and Automated Driving Systems (ADS). The most important reason for these accidents is that there are function decencies in robustness, generalization, interpretability, logical completeness, etc., those function decencies may cause the safety of the intended functionality (SOTIF) accident under a triggering condition. Introducing a new type of sensor may achieve the goal of producing more reliable information with less uncertainty. In this thesis, passengers' brain signals, including electroencephalography (EEG) and functional near-infrared spectroscopy (fNIRS), were analyzed to extract road information to potentially prevent car accidents and provide public trust in high-level autonomous vehicles. For the EEG part, event-related potential (ERP) and machine learning techniques were used to analyze and classify the signals of two road events: pedestrians standing on the curb and suddenly crossing the street. Results show that the responses are 454 ± 234 ms before the reaction, and the average recognition accuracy of the regularized linear discriminant analysis (RLDA) classifier reached 95.81%. For the fNIRS part, a quantification method, which is based on cerebral oxygen exchange in the prefrontal cortex of passengers and a risk field is introduced. We also verified our findings in a real-car automatic emergency braking (AEB) and cut-in experiment performed at China Automotive Engineering Research Institute (CAERI) automobile testing base in Dazu, China. Overall, the results illustrate that EEG-based human-centric assistant driving systems have the potential of being

deployed in high-level autonomous vehicles to enhance the safety of passengers and overall public safety.

Acknowledgments

The author would like to appreciate Dr. Mohamed Atia and Dr. Hong Wang for encouraging the author to investigate passengers' brain signals to enhance the safety of autonomous vehicles and for the supervision of this research, CAERI Intelligent Connected Technology Co., Ltd for providing the non-public track for the real-car experiment, and finally all the participants in the experiment.

The author would like to appreciate the financial support of the National Science Foundation of China Project: U1964203 and 52072215, National Key R&D Program of China: 2020YFB1600303, and Natural Sciences and Engineering Research Council (NSERC) of Canada, Discovery Grant: RGPIN-2017-06261.

Table of Contents

List of Tables

This is the List of Tables.

List of Illustrations

This is the List of Illustrations.

List of Appendices

This page lists all of the appendices.

List of Acronyms

ADAS: Advanced Driver Assistance Systems

ADS: Automated Driving Systems

AEB: Automatic Emergency Braking

ASR: Automated Artifact Rejection

CAERI: China Automotive Engineering Research Institute

CSP: Common Spatial Pattern

EDA: Electro-dermal Activity

EEG: Electroencephalography

EMG: Electromyography

ERP: Event-related Potential

fMRI: Functional Magnetic Resonance Imaging

fNIRS: Functional Near-infrared Spectroscopy

ICA: Independent Component Analysis

PCA: Principal Component Analysis

RLDA: Regularized Linear Discriminant Analysis

SOTIF: Safety of The Intended Functionality

SVM: Support Vector Machine

Chapter 1: Introduction

1.1 Background

With an increasing number of vehicles with automated functions on the road, Advanced Driver Assistance Systems (ADAS) is taking over more and more vehicle driving tasks. However, road safety is still one of the biggest concerns for autonomous vehicles. Multiple crash reporting for vehicles shows the limitations of sensors and algorithms on vehicles equipped with Advanced Driver Assistance Systems (ADAS) and Automated Driving Systems (ADS) [1], [2]. The most important reason for these accidents is that there are function decencies in robustness, generalization, interpretability, logical completeness etc., those function decencies may cause the safety of the intended functionality (SOTIF) accident under a triggering condition. The International Organization for Standardization (ISO 21448:2022) defines SOTIF, which is "the absence of unreasonable risk due to a hazard caused by: a. the insufficiencies of specification of the intended functionality at the vehicle level, or b. the insufficiencies of specification or performance limitations in the implementation of E/E elements in the system" [3]. One example of SOTIF scenarios is that a tesla autonomous vehicle hit a rollover white truck because the rollover white truck was mistakenly identified as white clouds [4]. Automatic driving systems must prevent potentially dangerous behaviors caused by the expected function or performance limitation of systems.

Multi-sensor fusion systems and advanced object-detection algorithms may reduce the amount of uncertainty to enhance the liability of the automated driving systems [5], [6]. It may solve the issue of sensor limitation under certain circumstances, such as glare that distorts video sensors, radar's poor vision abilities, the distance constraints of ultrasonic

sensors, lidar's inability to operate in inclement weather, etc. [7]. From a hardware perspective, introducing a new type of sensor may also achieve the goal of producing more reliable information with less uncertainty.

In recent years, some studies based on human status for autonomous vehicles have been done. Several physiological signals, such as electromyography (EMG), electrocardiogram (EKG or ECG), electro-dermal activity (EDA), eye movements, respiration, brain signals, etc., were collected and analyzed, aimed to potentially assists human drivers and reduce the rate of car accidents [8]–[11]. Among all these methods, monitoring brain activities is the best way to reflect human advanced cognition. A brain-computer interface (BCI) is a method that can allow humans to communicate with a computer or another electronic device using brain signals. Various methods can be utilized to monitor brain activities, e.g., magnetoencephalography, near-infrared spectroscopy (fNIRS), electroencephalography (EEG), and functional magnetic resonance imaging (fMRI) [12], [13]. Although both EEG and fNIRS have the advantages of relatively low cost and portability, EEG monitors brain activity faster and for a longer period than other methods, making it the most used method in BCI systems[13], [14]. Since fNIRS utilizes near-infrared to measure the change in cerebral blood flow (CBF) and related hemoglobin concentrations and EEG measures an electrical process, it is possible to use both devices together. EEG and fNIRS have been coupled to increase classification accuracy in several studies[15]–[18].

1.2 Contributions

In this thesis, passengers' brain signals, including electroencephalography (EEG) and functional near-infrared spectroscopy (fNIRS), were analyzed to extract road information to potentially prevent car accidents and provide public trust in high-level autonomous vehicles. For the EEG part, we analyzed passengers' EEG signals to distinguish between emergency and non-emergency events. 64-Channel EEG signals of 9 participants were collected when they were watching a simulated driving video with pedestrians standing on the right side of the road and suddenly crossing the street, from the front passenger seat point of view. Event-related potential (ERP) and machine learning techniques were used to analyze and classify the signals of two road events. Results show that the responses are 454 ± 234 ms before the reaction, and the average recognition accuracy of the regularized linear discriminant analysis (RLDA) classifier reached 95.81%. We also verified our findings in a real-car automatic emergency braking (AEB) experiment. It is the first study to investigate a passenger's EEG signals of emergency situations during simulated and real-world autonomous driving experiments. For the fNIRS part, a quantification method, which bases on cerebral oxygen exchange in the prefrontal cortex of passengers and a risk field, is introduced. Cerebral oxygen exchange was monitored by functional near-infrared spectroscopy, and autonomous emergency braking and cut-in experiments are performed in Dazu experimental base in China. There are two findings, one finding is that the Brodmann area 9 (BA 9) region is sensitive to risk change compared with other regions in the prefrontal cortex of passengers, and another finding is that in a certain range, driving scene risk rises may bring about cerebral oxygen exchange increase, and this provides a possibility for solving safety of the intended functionality by

using passengers' driving safety cognition. Overall, the results illustrate that EEG-based human-centric assistant driving systems have the potential of being deployed in high-level autonomous vehicles to enhance the safety of passengers and overall public safety.

We submitted two manuscripts for publishing, and both got accepted. For the EEG part of the research, we submitted to IEEE Intelligent Transportation System Conference[1], and for fNIRS, we submitted to the Automotive Innovation[2] journal. The information of both publications is listed below:

1. Fu, J., Zhang, X., Yu, W., Li, J., Atia, M., Wang, H.*, Li, C., Hao, Z. (2022) Decoding Passenger's EEG Signals from Encountering Emergency Road Events. In 2022 International Conference on Intelligent Transportation Systems (ITSC)
2. Zhang, X., Li, C., Li, J., Cao, B., Fu, J., Wang, H.*. (2022) The Passengers' Driving Risk Cognition Quantification in Prefrontal Cortex Based on fNIRS in High-Level Automated Vehicles. In Automotive Innovation

Chapter 2: Related Research

2.1 EEG

Previous research focused on drivers' behavior, stress level, mental workload, and intention, which can be detected and predicted based on EEG and some physiological signals, e.g., Electromyography (EMG), respiration, galvanic skin response (GSR)[11], [19]–[22]. Both Haufe et al. and Kim et al. proposed an ERP character including components for sensory registration of critical traffic situations[23], [24]. Bi et al. proposed a method that can generate braking command 293 ms earlier than an average behavioral response scheme, with a system accuracy of 94.89%, using spatial-frequency features[25], [26]. Vecchiato et al. discovered that theta power synchronization distinguishes braking from acceleration events 800 ms before the foot movement[27]. Khaliliardali et al. measured the contingent negative variation (CNV) and showed that the acceleration and brake intention can be predicted at 320 ± 200 ms before the action[28].

An EEG-based brain-computer interface usually contains 4 stages: data acquisition, preprocessing, feature extraction, and classification. The most discriminative part of the EEG signal processing is the feature extraction techniques. All the research now focused on the driver's status and required participants to control the real/simulated vehicles. They used different features extraction techniques to make the detection of brake intention faster. However, drivers may not be needed in a vehicle with a high-level autonomy. One thing in common is that the classification rate suffers from using one common model for all subjects. Results shows that training model for individual subject leads to a better classification result. Moreover, recent research are also lack of testing scenarios, which means the result could not summarize all the road events on the street.

2.2 fNIRS

Some research teams point out that fNIRS-measured prefrontal activity may discriminate cognitive states in real life[29], [30]. William J. Horrey explored the impact of task engagement on driving performance, subjective appraisals of performance and workload, and various physiological measurements and pointed out that the response time of driver to braking events is longer in the interesting audio condition[31]. Stephanie Balters investigated that the underlying mechanism of fNIRS limits its application and provided a collision that fNIRS is suitable to detect the driver habituation that is present when drivers operate new automated driving systems[32]. Yoshitomo Orino explored the relationship between cortical activation patterns and driving behaviors[33]. Liwei Xu investigated the mechanism of cooperation of different brain regions[34]. Jennifer L. Bruno discovered the states and traits of the brain may be helpful to predict the driver's response to changes in vehicle dynamics[35]. Anh Son Le illustrated that cognitive workload levels could be well classified through fNIRS data [36]. Kouji Yamamoto found that both the parietal association cortex and prefrontal area are activated when people are driving [33]. Christophe Jallais investigated the hemodynamic responses to visual simulation in driving and found an increase of OxyHb concentration in occipital areas during vehicle is controlled under manual pattern, which suggests more attention is needed for processing vision under manual pattern[37]. In Geissler et al. research, the mental workloads in the city environment and country environment, which require distinct demands, were measured by fNIRS, and they proposed that the right middle frontal gyrus might be a suitable region for the application of powerful small-area brain-computer interfaces[38]. In this research, the cerebral cortex activity mechanism of the

driver's brake intention was analyzed [39]. Huve et al. presented a brain-computer interface (BCI) that may analyze brain activity in real-time and deduce the current driving mode[40].

2.3 Limitations of the existing research

There are some shortcomings in these research. First, most of the current research are carried out on driving simulators rather than on actual roads. The driving simulator cannot reproduce all factors of actual roads and may provide a different experience compared to the real vehicle on the road. Moreover, all these research focused on the driver's status and required participants to control the real/simulated vehicles, however, drivers may not be needed in a vehicle with a high-level autonomy. These relative works using the fNIRS focus on distinguishing fatigue and mental workloads instead of passengers' driving safety cognition. Passengers' driving safety cognition for the driving environment may help automatic driving systems prevent potentially dangerous behaviors caused by the expected function or performance limitation of systems. To simulate a high-level autonomy, the experiment was designed to avoid any actions such as pressing the brake pedal but only pressing the button to reflect the intention. In this work, we investigated neurophysiological signals and expected them to reflect the different road events.

Chapter 3: Methodology

In this chapter, the methods of processing and analyzing EEG and fNIRS signals will be explained in separate sections.

3.1 EEG Part

EEG stands for electroencephalogram, which records brain activity. Small sensors are affixed to the scalp during this painless examination to collect the electrical signals generated by the brain [41]. There are several ways to utilize EEG signals that pick up by amplifiers. ERP and machine learning approaches are used in this study. An event-related potential is an electrophysiological response to a specific stimulus. Different stimuli can trigger a variety of brain potentials. The electrophysiological response needs to be recorded multiple times and averaged for eliminating noise[42]. ERP can be utilized to investigate several questions. The common questions that were considered in this research are as follows: 1) Is there a difference in terms of brain response when the passenger encounters an emergency road event or normal driving? 2) Which region is corresponding to braking intention?. To conduct this research and to provide answers to these questions, physical experiments have been done and a machine learning method is introduced after we found a passenger's brain responses are different for different road events. The objective is to investigate if machines can classify two different potentials and the accuracy of the classification result.

3.1.1 System Architecture

Illustration 1 demonstrates the signal flow chart of the system including three parts: signal acquisition and preprocessing, ERP response analysis, and the machine learning approach. The signal flow chart shows the procedures of signal processing. After pre-

processing (including filtering, down-sampling, and independent component analysis (ICA) and automated artifact rejection (ASR)) and segmenting the signal, the ERP process shows the relation between EEG signals and road events, and machine learning models return the classification result of the system.

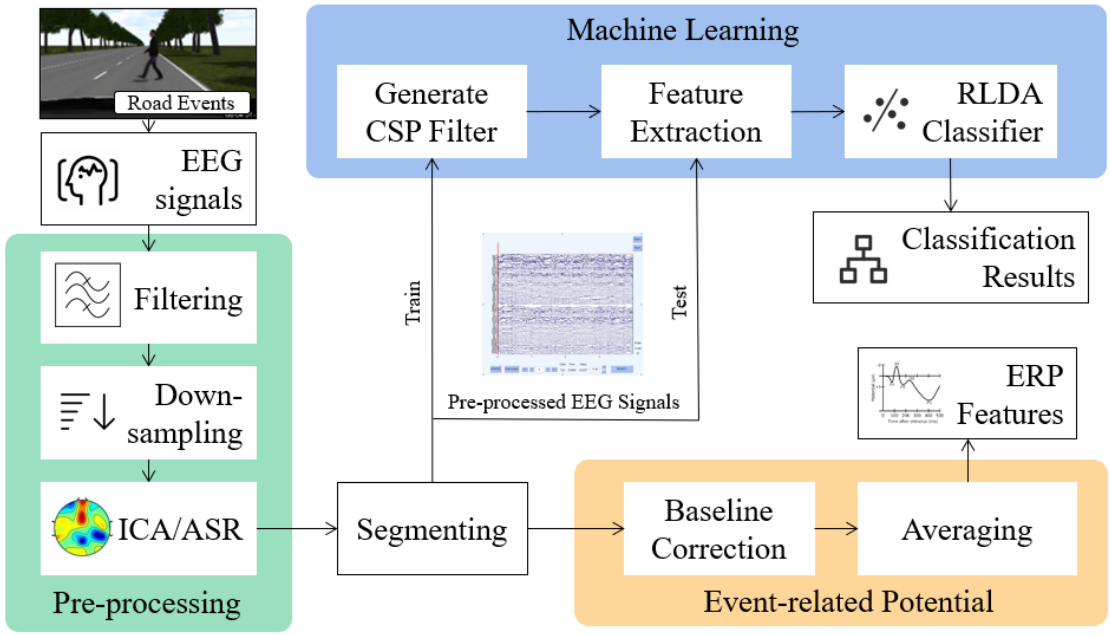

Illustration 1 EEG Signal flow chart

3.1.2 Data acquisition and preprocessing

EEG was acquired at 4000 Hz sampling frequency from 64 scalp sites based on an international 10–20 system, as shown in Fig. 2, using an EEG cap with Ag/AgCl electrodes (TMSi, Netherlands). A detailed introduction and spec. of the EEG hardware is described in Appendix B. The mean value of the two electrodes behind the ears (M1 and M2) was set as the reference. The impedance of each channel was below 30 kΩ. The EEG signals were amplified and digitized using SAGA 64+ hardware (TMSi, Netherlands).

MATLAB (MathWorks, US) and EEGLAB were used for the processing and analysis of all EEG signals. EEGLAB is an open-source toolbox of MATLAB for EEG signal processing. To eliminate signal drift, high-frequency distortions, and power-line noise, EEG signals were filtered with a 0.5 Hz to 60 Hz bandpass filter and a 50 Hz notch filter. EEG data were down-sampling to 1000 Hz. Independent component analysis (ICA) and Automated artifact rejection with Clean Raw data were used to remove ocular and muscle artifacts from EEG signals. EEG epochs were extracted based on the event start time in the video. The time range of each epoch was from 1-second pre-stimulus to 2 seconds post-stimulus for each event, with baseline correction before averaging.

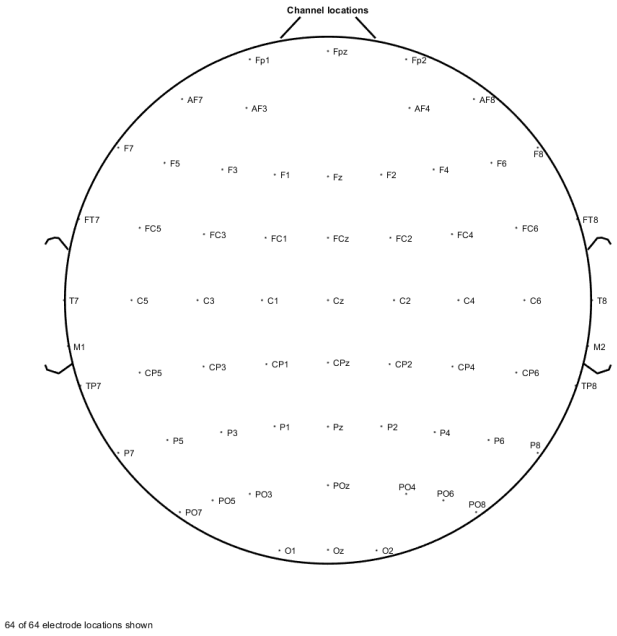

Illustration 2 Channel Locations of the collected EEG signals[43]

3.1.3 ERP study

The baseline correction step was applied to each epoch for the ERP response study to isolate the true spectroscopic signal from the interference effect and remove background

effects. Then we took the average of 40 trials of EEG signals of the pedestrian crossing event. Power spectral density of four frequency bands was calculated and topographical maps were plotted to find the cortex area that was involved in road events.

3.1.4 Feature extraction and classification

In the feature extraction part, the common spatial patterns (CSP) method was used to generate features or virtual channels that may distinguish the EEG signals of two events. We first used training data to generate a CSP filter, then used the CSP filter to transform the original EEG data into features for further classification. The number of feature pairs was tested to ensure the best performance of the classifier. The time range of each trial was 1 second before and after the stimulus event, which was before the average time the subjects pressed the button. In the classification part, RLDA was selected as the classifier.

3.1.4.1 Common Spatial Pattern (CSP) Filter

Common Spatial Pattern (CSP) is a spatial filtering feature extraction algorithm for two-class classification tasks, that was proposed by Koles et al. for EEG signal analysis [44]. CSP can extract the spatial distribution components of each class from multi-channel EEG signals. The basic principle of the CSP algorithm is to use the diagonalization of the matrix to find a set of optimal space filters for projection, maximize the difference in the variance values of the two types of signals, and obtain the eigenvectors with higher discrimination.

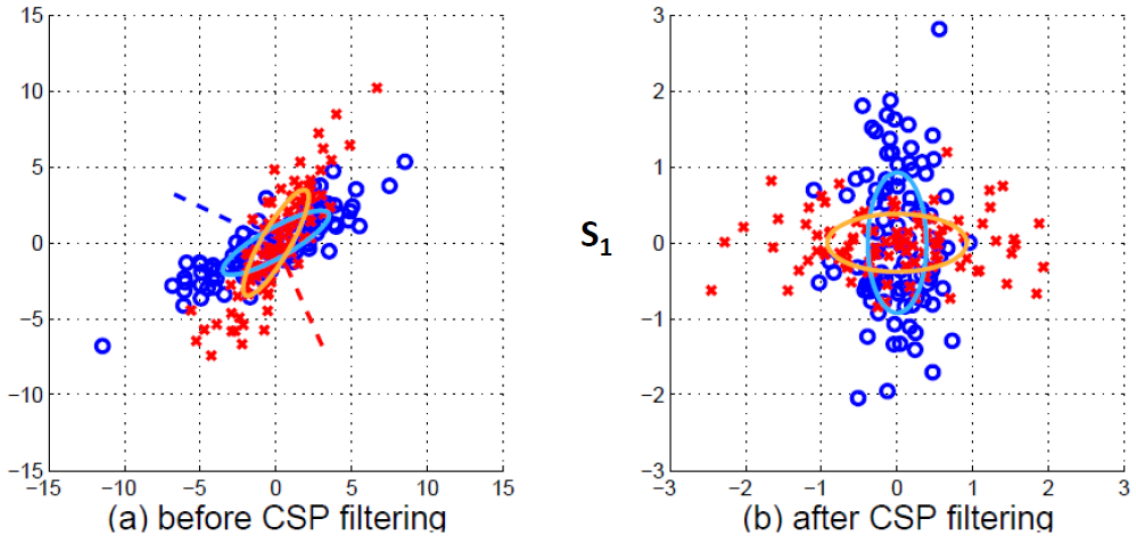

Illustration 3 Before and After CSP filtering of 2 Channels of EEG signal [45]

Suppose X_1 and X_2 are the multi-channel ERP spatial-temporal signal matrices under the two-class events, respectively. The dimensions are $N * T$, where N is the number of EEG channels, and T is the sample size of each channel. To calculate its covariance matrix, we assume that $N < T$, and the noise of EEG is ignored since the signals were pre-processed. X_1 and X_2 can now be written as:

$$X_1 = [\, C_1 \; C_M] \begin{bmatrix} S_1 \\ S_M \end{bmatrix}, X_2 = [\, C_2 \; C_M] \begin{bmatrix} S_2 \\ S_M \end{bmatrix}$$

(1)

In the equations, S_1 and S_2 represents the two different events. Assuming two events are linear-independent of each other, S_M represents the source signals that are shared by the two events. If S_1 and S_2 is composed of m_1 and m_2 number of sources, then C_1 and C_2 are composed of m_1 and m_2 number of common spatial patterns that related to S_1 and S_2. Since each spatial pattern is a vector with a dimension of $N * 1$, the vector can represent the distribution weight of the signal on N leads. C_M represents a common spatial

pattern corresponding to S_M. The goal of the CSP algorithm is to design the spatial filters F1 and F2 to obtain the spatial factor W.

To obtain the mixed spatial covariance matrix of two types of events, the normalized covariance matrices R_1 and R_2 need to be calculated:

$$R_1 = \frac{X_1 X_1^T}{trace(X_1 X_1^T)}, \qquad R_2 = \frac{X_2 X_2^T}{trace(X_2 X_2^T)} \tag{2}$$

$$R = \bar{R}_1 + \bar{R}_2 \tag{3}$$

where $\bar{R}_i$ is the average covariance matrix of each event.

Then apply principal component analysis (PCA) to find the whitening eigenvalue matrix P:

$$R = U \lambda U^T \tag{4}$$

where U is the eigenvector matrix of the matrix λ, λ is the diagonal matrix of the corresponding eigenvalues. Arrange the eigenvalues in descending order, and the whitening value matrix is:

$$P = \sqrt{\lambda^{-1}} U^T \tag{5}$$

To form the spatial filter, R_1 and R_2 are transformed as follows:

$$S_1 = P R_1 P^T, S_2 = P R_2 P^T \tag{6}$$

Then applied PCA to S_1 and S_2:

$$S_1 = B_1 R_1 {B_1}^T, S_2 = B_2 R_2 {B_2}^T$$

(7)

From equations 6 and 7:

$$B_1 = B_2 = V$$

(8)

At the same time, the sum of the diagonal matrix of eigenvalues, λ_1 and λ_2, is equal to identity matrix.

$$I = \lambda_1 + \lambda_2$$

(9)

That leads to the fact that the eigenvector corresponding to the largest eigenvalue of S_1 makes S_2 the smallest eigenvalue, and vice versa. Arrange the eigenvalues in λ_1 in descending order, then the corresponding eigenvalues in λ_2 are arranged in ascending order. According to this, it can be inferred that λ_1 and λ_2 have the following forms:

$$\lambda_1 = diag(I_1 \ \sigma_M \ 0),\ \lambda_2 = diag(0 \ \ \sigma_M \ I_2)$$

(10)

The transformation of the whitened EEG signal to the eigenvector corresponding to the largest eigenvalue in λ_1 and λ_2 is optimal for separating the variances in the two signal matrices. The projection matrix W is the corresponding spatial filter as:

$$W = B^T P$$

(11)

3.1.4.2 Feature extraction

The training dataset is used to form the CSP filter, then feature Z_1 and Z_2 can be extracted as:

$$Z_1 = W \times X_1, \qquad Z_2 = W \times X_2$$

(12)

According to the definition of the feature extraction of EEG signals collected by the CSP algorithm in multi-electrode, this study selects f_1 and f_2 as the feature vectors of pedestrian crossing events and pedestrian non-crossing events, which are defined as follows:

$$f_1 = \frac{VAR(Z_1)}{sum(VAR(Z_1))}, \; f_2 = \frac{VAR(Z_2)}{sum(VAR(Z_2))}$$

(13)

3.1.4.3 Regularized Linear Discriminant Analysis (RLDA)

Regularized Linear Discriminant Analysis (RLDA) model was selected to classify EEG signals of two road events. Discriminant Analysis can be used as a classification and dimensionality reduction technique[46]. Linear Discriminant Analysis (LDA) and Quadratic Discriminant Analysis (QDA) is usually compared with RLDA. For a two-class classification problem, LDA is aimed at: the data following a Gaussian distribution, the mean is different, and the variance is the same. Meanwhile, QDA is aimed at: the data following a Gaussian distribution, and the mean and the variance are different[47]. As a compromise between LDA and QDA, RLDA was developed, and it has the benefit of dealing with a large number of features [46]. In this research, we are using 20 to 34 pairs of features, and the sample size is relatively small. After comparing with the

classification result of an support vector machine (SVM) classifier, we choose the RLDA classifier to achieve the event classification task.

3.2 fNIRS Part

A blood oxygen monitoring device can measure concentration changes of oxy-hemoglobin and deoxy-hemoglobin based on the scattering (light diffusing) properties of tissue by fNIRS, in which each data acquisition channel is formed by an emitter and a receiver [48], [49]. The blood oxygen monitoring device adopted in this experiment shown in illustration 4, is named OctaMon+ provided by Artinis, a Dutch NIRS company. The device relies on continuous wave near-infrared spectroscopy with improved Lambert-Beer law. There are two wavelengths for a light source, 760nm, and 850nm, and the distance between two optodes is 30mm. The device has 8 channels with a sampling frequency of 50Hz, and the measurement region is located in the prefrontal cortex. When attaching probes, each optode is adjusted to ensure good signal quality.

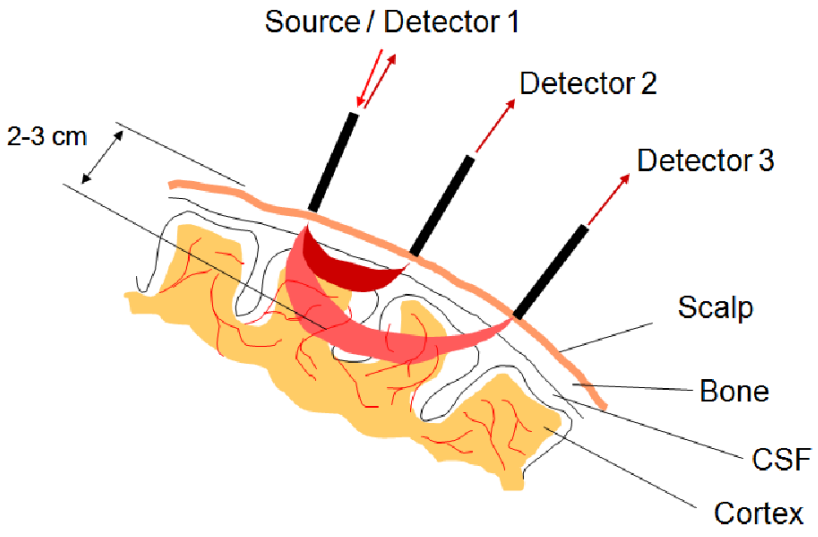

Illustration 4 Principle of fNIRS

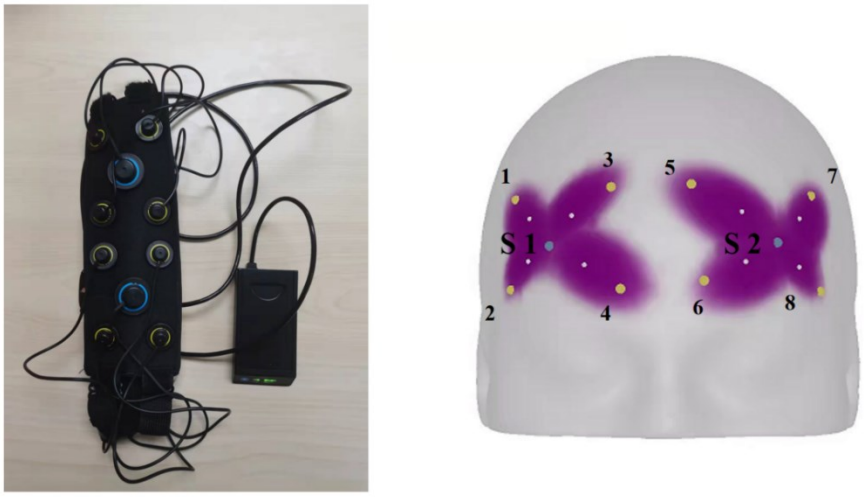

Illustration 5 OctaMon+ device and its location of the 3D model

3.2.1 System architecture

The experiment design was described in illustration 6. We first designed two experiment scenes: advanced emergency braking (AEB) and cut-in of the high-speed cruise (HWP), and invited volunteers to participate in these experiments, the whole experiments were performed in the Dazu experimental base in China. During those experiments, UFO equipment (an inflated vehicle system provided by CAERI Intelligent Connected Technology Co., Ltd.) recorded driving data including speed and acceleration, and blood oxygen monitoring equipment based on fNIRS recorded passengers' cerebral cortical activity data, including the change concentration of deoxy-hemoglobin and oxy-hemoglobin. Then, the driving data and the cerebral cortical activity data were synchronized by time, and a kinetic energy field, which represents a driving scene danger degree, and cerebral oxygen exchange were calculated by the collected data. Finally, we analyzed the relationship between the kinetic energy field change and cerebral oxygen

exchange change and figure out the sensitive area of the passenger and a quantitative passenger's driving safety cognition way.

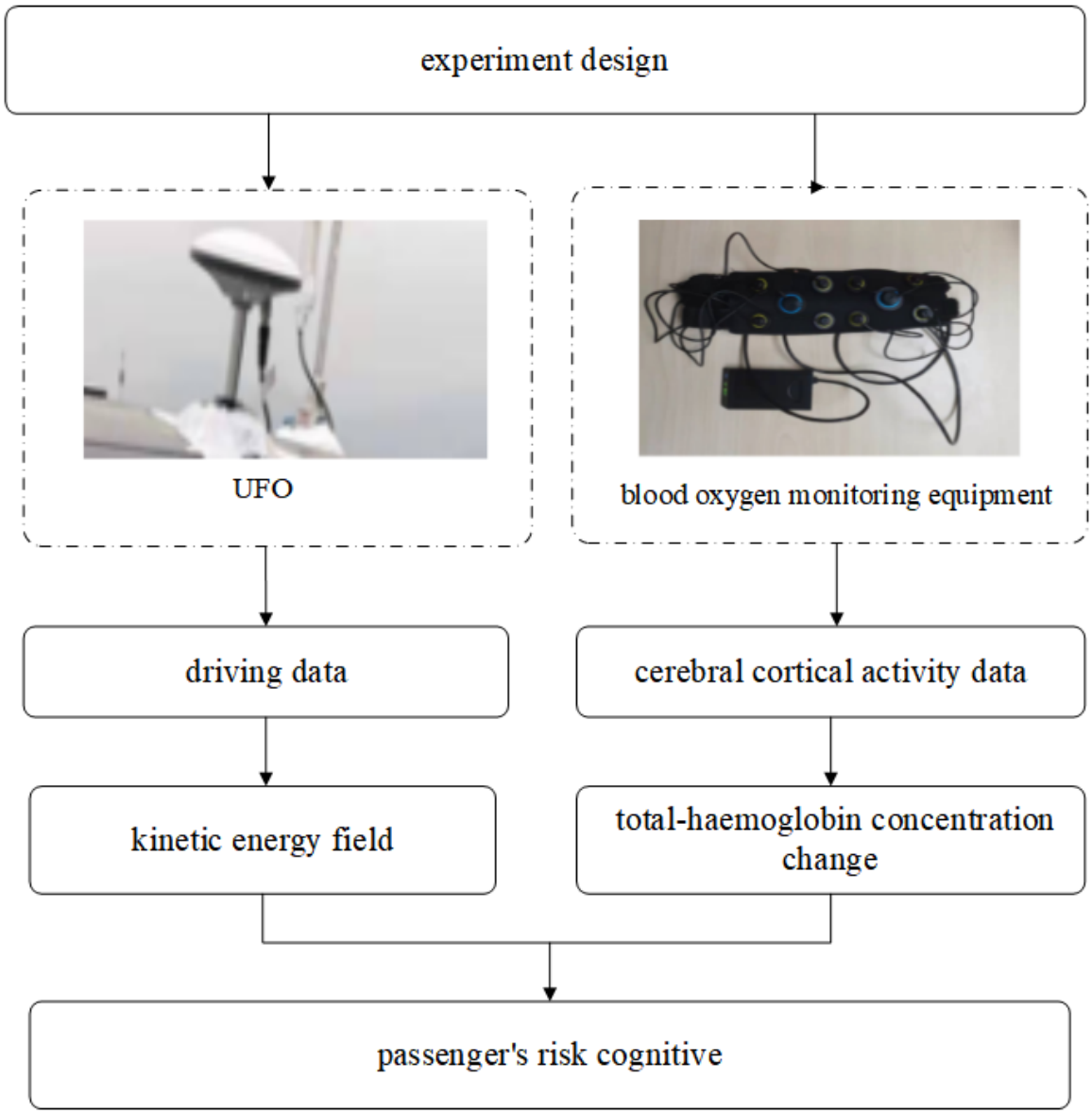

Illustration 6 System Architecture

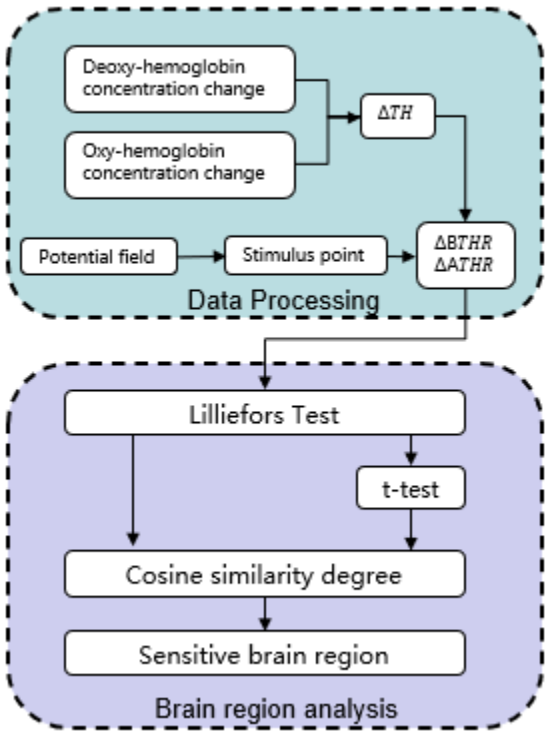

Illustration 7 Data processing procedure

The data processing procedure can be divided into three parts: data preprocessing process, sensitive brain region analysis for risk change, and quantification of passengers' driving safety cognition.

3.2.2 Data preprocessing

The data, which are obtained by blood oxygen monitoring equipment based on fNIRS, are processed with a MATLAB toolkit: Homre3. Firstly, we convert intensity data to optical density using the *hmrR_Intensity2OD* function. Secondly, the low-frequency characteristics and outliers of optical density data are removed by a lowpass filter with a cut-off frequency of 0.5 Hz. Finally, changes in HbO_2 and HHb relative to the initial baseline is calculated using the *hmrR_OD2Conc* function.

3.2.3 Risk field calculation

In this work, we consider the kinetic energy field, which is caused by the moving target vehicle, and the kinetic energy may indicate a dangerous degree of driving scene. The kinetic energy can be calculated by using data which are obtained by sensors on the target vehicle[50],

$$E_v = \frac{GR_2M_2}{r^{k_1}} \frac{r^{k_1}}{|r^{k_1}|} e^{[k_2 v_2 \cos(\theta_2)]} \quad (14)$$

where k_1, k_2, G are three positive constants, M_2 indicates target vehicle mass, r indicates the distance between target vehicle and ego vehicle, v_2 represents target vehicle speed, R_2 is the road impact factor, and θ_2 indicates the angle between r and v_2. Illustration 8 is a sketch map of E_v, in which $\theta_2 = 0$, and $v_2 = 50$ km/h.

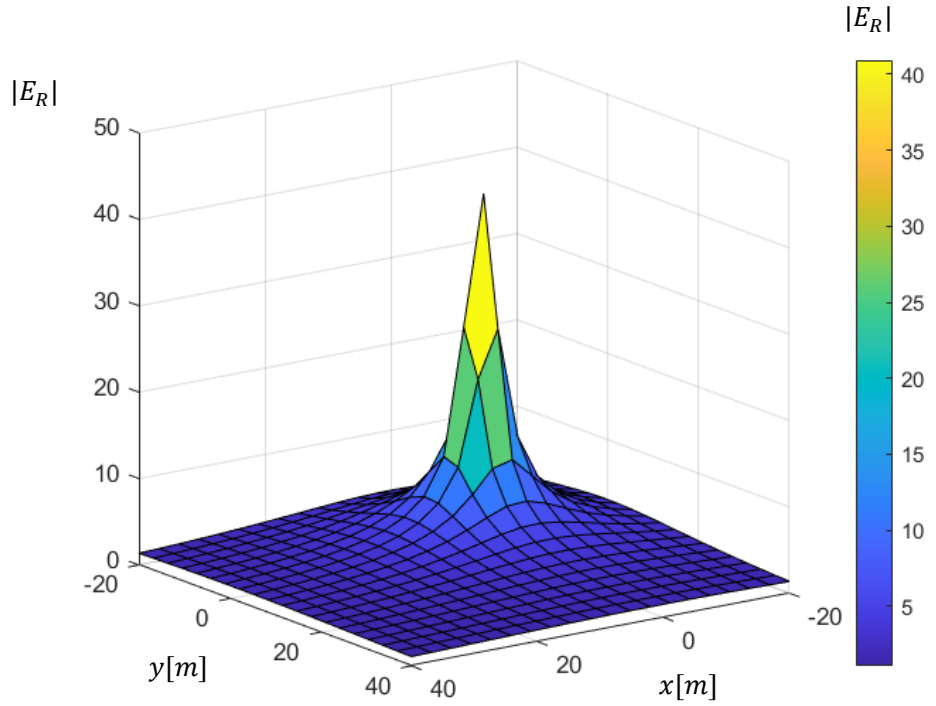

Illustration 8 Kinetic energy field when v_2 = 50 km/h

The moment when the risk field begins to rise, which means the ego car encounter a dangerous driving scene, is defined as a stimulus point. In this work, we calculate the derivative of the risk field and take the moment in which the risk field derivative is maximum as a stimulus moment.

$$\frac{dy_i}{dt_i} = \frac{\Delta y}{\Delta t} = \frac{y_{i+1} - y_i}{t_{i+1} - t_i}$$

(15)

Previous studies have shown that cerebral oxygen exchange ΔTH is an effective index, which may indicate brain activity[51]–[53]. In this work, we choose ΔTHR (ΔTH range, i.e., the difference between the ΔTH's maximum and the ΔTH's minimum in a time window) as an index, which reflects the intensity of cerebral cortex activity. We compared $\Delta \mathrm{B}THR$ and $\Delta \mathrm{A}THR$ ($\Delta \mathrm{B}THR$ indicates the ΔTHR 2 seconds before the stimulus moment, and $\Delta \mathrm{A}THR$ indicates the ΔTHR in 2 seconds after stimulus moment).

$$\Delta TH = \frac{\Delta HHb - \Delta HbO_2}{\sqrt{2}}$$

(16)

3.2.4 Sensitive brain region analysis for risk change

Lilliefors test was adopted to test data distribution and sort data according to whether it follows a normal distribution. Then t-test was adopted to detect the difference between $\Delta \mathrm{A}THR$ and $\Delta \mathrm{B}THR$, which follow a normal distribution and find the channel in which the *p*-value is minimum.

The cosine similarity algorithm was used to calculate differences in those channels to find data that don't follow a normal distribution. A cosine similarity algorithm is a way to measure the difference between two samples using the cosine of the angle between two

vectors in vector space. The vector similarity degree is judged by the angle magnitude. The channel corresponding to the largest cosine value is selected as a sensitive channel to passengers' driving safety cognition.

$$\cos(\theta) = \frac{\mathrm{X} \cdot \mathrm{Y}}{\|X\|\|Y\|} = \frac{\sum_{i=1}^{n}(x_i \times y_i)}{\sqrt{\sum_{i=1}^{n}(x_i)^2} \times \sqrt{\sum_{i=1}^{n}(y_i)^2}} \quad (17)$$

To find the relationship between cerebral oxygen exchange change and risk field change, and quantify passengers' driving safety cognition, we first calculated the difference of mean kinetic energy field in 2s between pre-stimulus and post-stimulus for indicating the risk difference degree. Then, the cosine similarity degree of ΔTH in 2s between pre-stimulus and post-stimulus were calculated for the change degree of the passenger's brain state. Finally, we analyzed a quantification index of the passenger's driving safety cognition-based information we got from previous steps.

3.3 Experimental Design

3.3.1 EEG Pedestrian Crossing Experiment

3.3.1.1 Participants

The first stage of the experiment involved a total of 9 individuals. Due to technical issues, one of the obtained datasets had to be eliminated from further study. As a result, the sample consisted of eight men (23-32 years, mean: 25.7 years). All the subjects had normal or corrected-to-normal eyesight and hearing, as well as no history of psychiatric or neurological illnesses. In terms of driving experience, all participants were either lack of a driver's license or inexperienced behind the wheel. Before taking part in the experiment, none of the participants had consumed any drugs, tobacco, alcohol, or caffeine. The participation was completely voluntary and took place during working hours. Data were collected anonymously. EEG signals of participants have collected anonymously. The ability to withdraw from the experiment at any moment without incurring any penalties was made clear to participants.

3.3.1.2 Experimental setup

The participant was asked to sit in front of a screen and watch a video of a virtual car driving on a road at a speed of 60 km/h, as shown in illustration 9. The video is generated by Virtual Test Drive (VTD) software with a first-person point of view from the front passenger seat. Two types of events, a pedestrian crossing the street or standing on the right side of the street as shown in illustration 10, happened with random orders each 20-30 seconds during the entire 30 mins video. The vehicle was set to autonomous mode, which will suddenly slow down when the pedestrian is too closed. For the pedestrian

crossing scenario, the pedestrian will start crossing at a speed of 10 km/h, 35 m away from the vehicle. There are in total of 40 pedestrian crossing events and 33 pedestrian standing events. The participants were instructed to press a button when they observed pedestrian sudden crossings. For all the participants, since there is no actual driving involved but only pressing buttons, there was no training needed before the experiment.

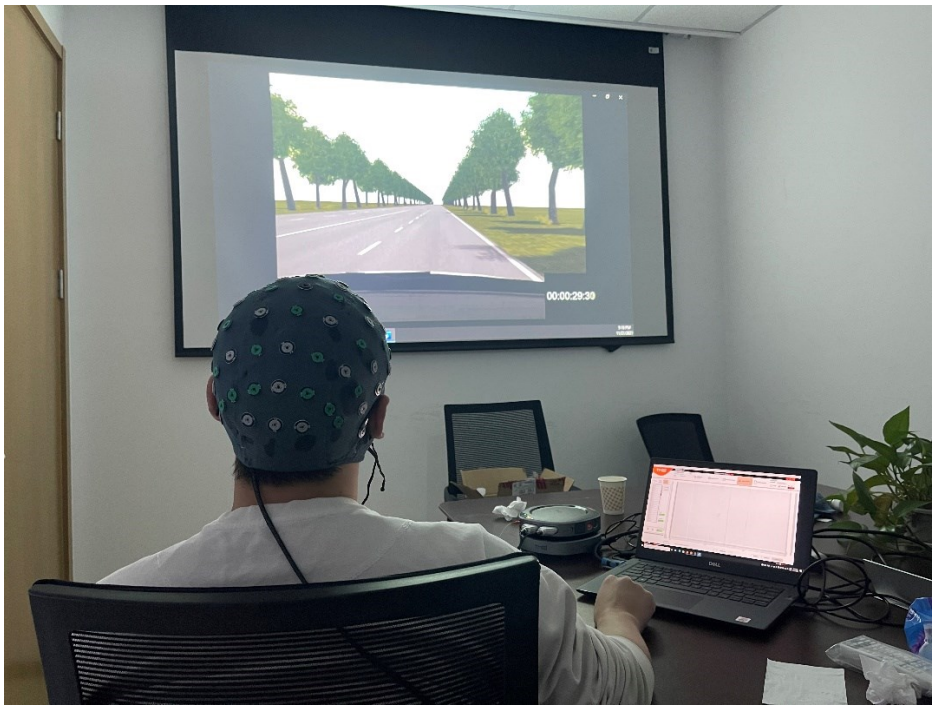

Illustration 9 Experiment Setup for VTD experiment

Illustration 10 Scenarios of the experiment: a pedestrian suddenly crossing

Illustration 11 Scenarios of the experiment: a pedestrian standing on the right side of the road

3.3.2 Real-car experiment

3.3.2.1 Participant

For the real-car EEG experiment, one individual at the age of 23 participated in this experiment. Informed consent was obtained after the task had been explained. The same EEG hardware and data acquisition techniques as the VTD experiment were used in this test. All setups were performed by the same research personnel as in the previous experiment to ensure the participant's safety and EEG signals' quality. For all the participants, since there is no actual driving involved but only pressing buttons, there was no training needed before the experiment.

Illustration 12 The subject for the real-car experiment

3.3.2.2 Experimental setup

The experiment was conducted on a non-public test track in China's Automotive Engineering Research Institute (CAERI) automobile testing base in Dazu, Chongqing. The setup consisted of two vehicles: an inflatable car towed by a pick-up truck as the lead car followed by a Mercedes-Benz C-Class car with adaptive cruise control (ACC) and AEB function. Both vehicles were running at a speed of 40 km/h 15 m apart. After an instruction sent by the following car, the lead car's driver randomly started braking from 40 km/h to 0 km/h, which triggered the AEB function of the following car. The participant was asked to pay attention to the road without any actions such as braking or pressing a button.

Illustration 13 China Automotive Engineering Research Institute (CAERI) automobile testing base

Illustration 14 Real-car Experiment Setup

3.3.3 fNIRS Experiments

3.3.3.1 Experiment Instrument -- UFO

UFO is a system provided by CAERI Intelligent Connected Technology Co., Ltd. It contains a fake car, which can be used as the target vehicle in the ADAS test, and the motion parameters of the ego vehicle and target vehicle can be obtained by UFO, such as speed, acceleration, etc. Relative parameters can also be obtained by UFO, such as relative longitudinal distance, relative lateral distance, and relative speed, and the track and speed of the target vehicle can be adjusted by UFO, which makes it can simulate a real vehicle. UFO can be used in some dangerous scenes during testing, such as AEB, cut-in, cut-out, etc.

UFO works as shown in illustration 15. An inertial navigation system, a driving robot, and a communication module are installed on the ego vehicle. The soft collision target is placed on the mobile chassis to form the target vehicle, and the controller is placed under

the vehicle. UFO is connected with the ego vehicle through the combination of the inertial navigation system, communication module, and controller. The information about other vehicles is sent to a controller through the communication module. The controller updates vehicle position information by using differential signals and sends updated information to the CPU in the chassis, the relative speed and relative distance of two vehicles are calculated by the CPU. Messages are sent to the ego vehicle to exchange data between the ego vehicle and target vehicle and control the chassis at the same time.

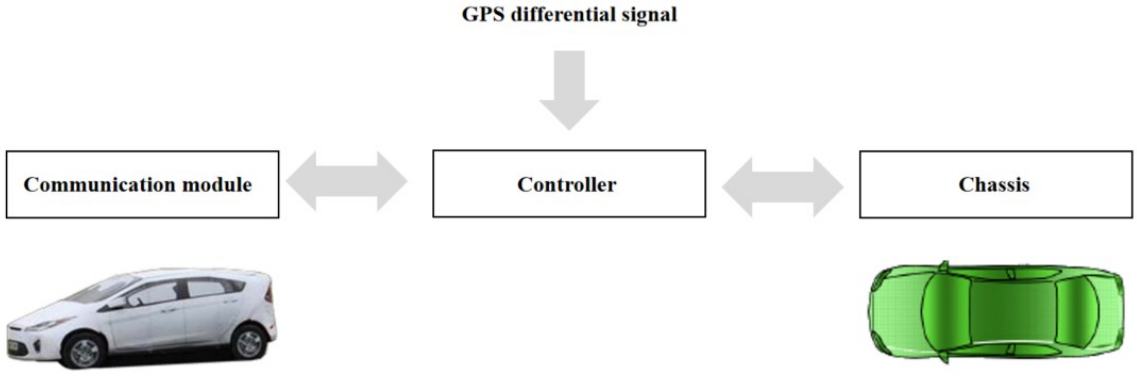

Illustration 15 The working process of UFO

3.3.3.2 Experiment Setup

The experiment was conducted on a non-public test track in China's Automotive Engineering Research Institute (CAERI) automobile testing base in Dazu, Chongqing. Two subjects are tested in this experiment, and they are shown in illustration 16. One subject sat in the driver seat (34 years old) and blood oxygen monitoring equipment was attached to the subject's forehead in a way that for allowing measure concentration changes, the other subject sit at the co-pilot’s seat and the electroencephalogram equipment was attached to the subject's head. The subject who sat in the driver's seat did

not need to operate the automated vehicles and was considered a passenger. We took 16 group tests for the AEB scene and 9 group tests for the cut-in scene. The participants are volunteers, informed consent was obtained after the task had been explained, and participants were informed that they have an option to end participation in this experiment at any time without any type of penalty.

Illustration 16 The subject for the real-car experiment

3.3.3.3 Experiment Scenes

3.3.3.3.1 Advanced Emergency Braking Scene

The setup consisted of two vehicles: an inflatable car towed by a pick-up truck as the lead car followed by a Mercedes-Benz C-Class car with adaptive cruise control (ACC) and AEB function. Both vehicles were running at a speed of 40 km/h 15 m apart. After an instruction sent by the following car, the lead car's driver randomly started braking from 40 km/h to 0 km/h, which triggered the AEB function of the following car.

3.3.3.3.2 Cut in of Highway Pilot Scene

In this scene, a male subject (23 years old) also sits in an ego vehicle. UFO's moving trajectory and speed were set, which is shown in illustration 17. When the ego vehicle reached the desired speed, the ACC function was turned on. The fake car will switch to this lane from the left lane at different speeds and different distances.

Illustration 17 HWP Cut-in Scene

Chapter 4: Results

4.1 EEG Experiment Results

4.1.1 ERP Analysis

We took an average EEG signal of 40 trials of a pedestrian crossing the street and 33 trials of a pedestrian standing on the sidewalk for each subject. Before we analyzed the ERP response, the reaction time can be observed during the test. Then, by analyzing the ERP response, two features can be observed, and one example of a subject is shown in illustrations 18 and 19. ERP responses of other participants are shown in Appendix C. The stimulus onset (STMI) at 0 ms means that the pedestrian starts to cross the street at this point, and it is the point when the pedestrian lifts his foot. The first feature was before the stimulus onset. It was because participants can spot the pedestrian standing at the side of the road from a decent distance. After analyzing the ERP for all the subjects, the second feature can be found at an average of 454 ± 234 ms before the response, which was related to the action of pressing the button.

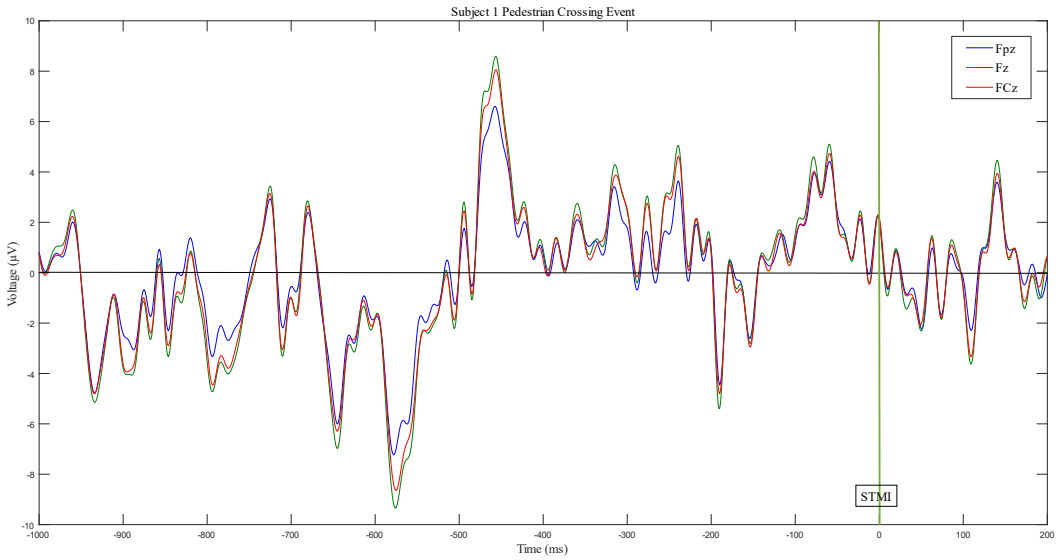

Illustration 18 ERP response of three EEG channels (Fpz, Fz, FCz) from -1000 ms to 200 ms

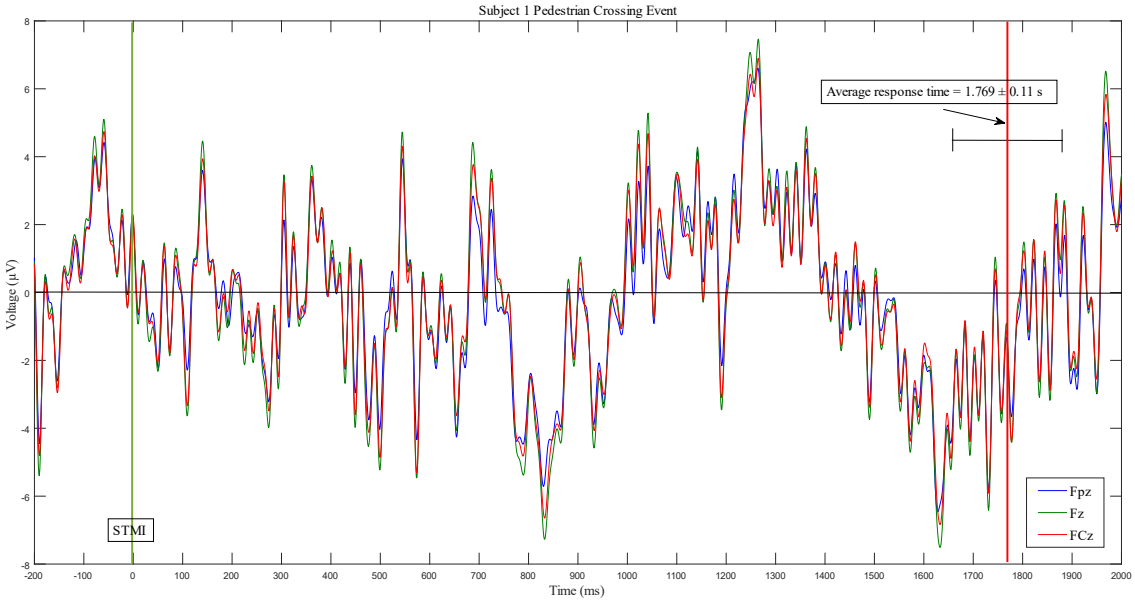

Illustration 19 ERP response of three EEG channels (Fpz, Fz, FCz) from -200 ms to 2000 ms

Table 1 Participants' performance model

Participants	Reaction Time (s)	Perception + Decision Time (s)	Action Time (s)
Subject 1	1.769	1.2650	0.5040
Subject 2	1.616	1.1114	0.5020
Subject 3	1.212	0.7480	0.4640
Subject 4	1.117	1.0020	0.1150
Subject 5	1.511	0.6000	0.9110
Subject 6	1.473	0.9500	0.5230
Subject 7	1.239	0.7600	0.4790
Subject 8	1.135	1.0310	0.1300
Average	1.384	0.9340	0.4540

Table 1 shows the important time we found during the test. To calculate the action time, we set a threshold for any amplitude changes that are more than ± 6.5 μV. After comparing with the skilled human driver performance model in UN Regulation No. 157 - Automated Lane Keeping (in Appendix 1), we found that our result matches their experiment results.

Illustrations 20 and 21 show the topographical maps of grand-average AUC scores calculated from ERP for theta-band (6 Hz), alpha-band (10 Hz), beta-band (22 Hz), and gamma-band (40 Hz) from -1000 ms to 200 ms and -200 ms to 2000, which indicated the cortex area that was involved in road events.

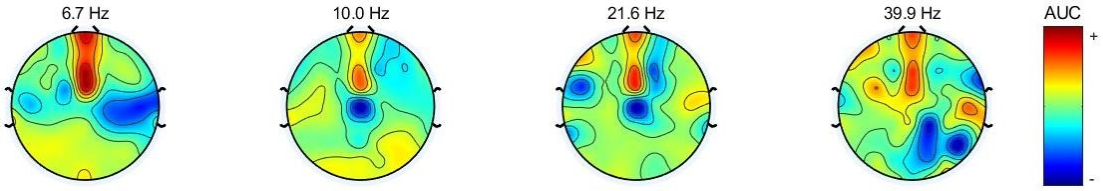

Illustration 20 Topographical maps of four frequency bands from -1000 ms to 200 ms

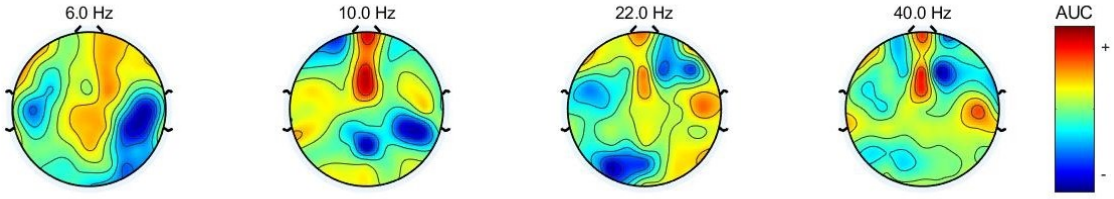

Illustration 21 Topographical maps of four frequency bands from -200 ms to 2000 ms

4.1.2 Machine Learning Method Evaluation

We added 40 trails of EEG data of normal driving periods as non-crossing events. The normal driving events were selected in between any other road events, including pedestrian crossing and non-crossing, and we avoided selecting the normal driving time interval that was close to those two events. By generating the CSP filter matrix using EEG signals, we can get a CSP filter with a dimension equal to the number of channels. Then the features can be generated using the training and testing EEG data. Illustration 22 shows two extracted features of the two events. Twenty pairs of features were extracted from the preprocessed EEG signals of each subject. Then we applied 10-fold cross-validation to evaluate the classifier. Fig. 7 shows the classification accuracy for each subject and the average classification accuracy, which is 95.81%. Then, we used EEG signals from all subjects to train and test the classifier. The required number of features increased to 34 pairs to meet the maximum classification accuracy of 76.37%.

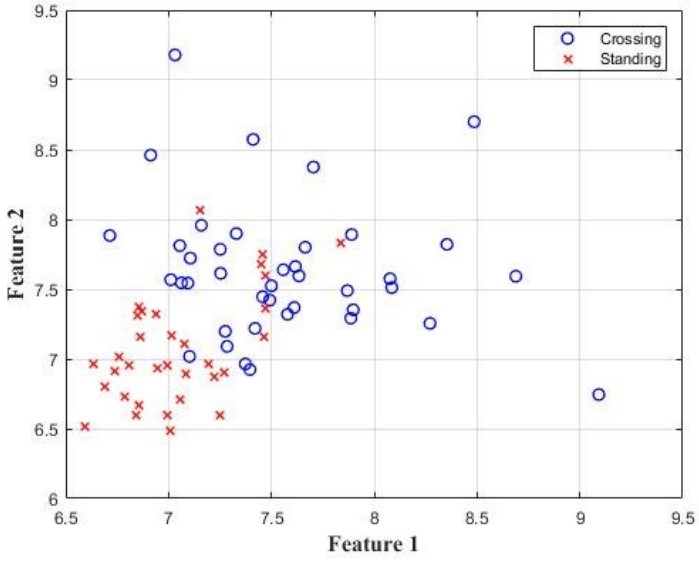

Illustration 22 Two extracted features/channels of each road event

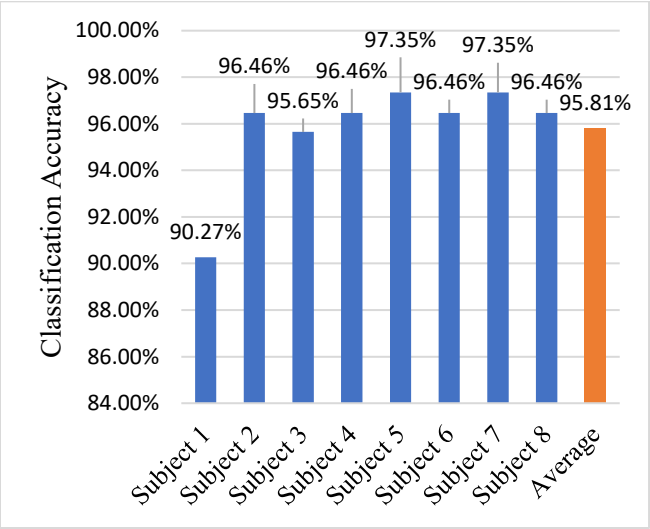

Illustration 23 Classification performance of all participants

4.1.3 Real-car Experiment ERP Analysis

There were in total of 15 trials of the experiment conducted. EEG signals were processed using the same procedures in the VTD experiment. Two features can be found in the ERP response before the AEB function braking the vehicle as shown in Illustration 24. Two features are shown in the Illustration. The first feature was related to the stimulus of the braking of the lead car. The second feature reflected the brake intention of the passenger due to the fast-decreasing distance between two vehicles. This shows that EEG signals of a passenger can reflect the emergency road event and be utilized to control the vehicle in an emergency situation to prevent collisions.

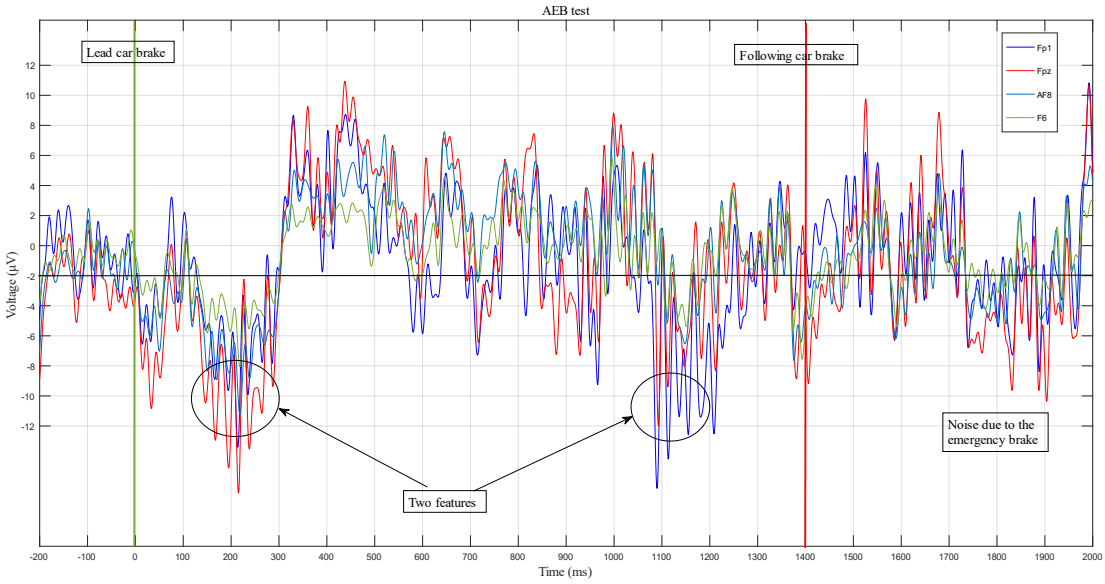

Illustration 24 ERP response for AEB experiment

4.2 fNIRS Experiment Results

4.2.1 AEB Results

Two trials of the AEB test were excluded because the data are not recorded correctly. The result of the Lilliefors test is shown in Table 2.

Table 2 The distribution result of the data △BTHR and △ATHR in the AEB experiment

data \ channel	1	2	3	4	5	6	7	8
$\triangle ATHR$	0	0	0	0	1	0	0	0
$\triangle BTHR$	0	0	0	0	0	0	1	0

0 indicates that data follows normal distribution, and 1 otherwise.

The result of Table 2 shows that the data of channels 1,2,3,4,6,8 follows a normal distribution. T-test was adopted to find the difference in probability of $\Delta BTHR$ and $\Delta ATHR$ in those channels. The small p value means a large difference in probability. The p values are shown in Illustration 25, and the p value of channel 4 is the minimum.

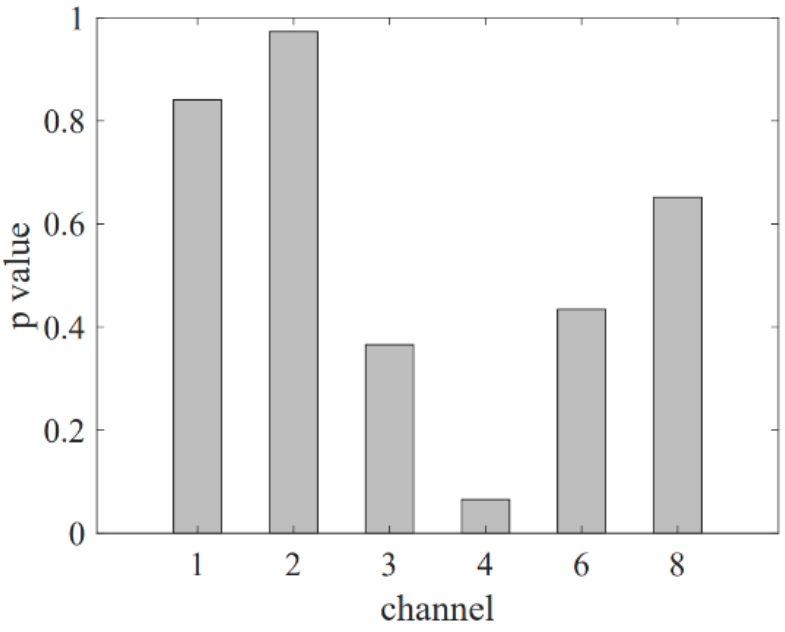

Illustration 25 The *p*-value for the fNIRS AEB test

The result in Table 2 shows that channel 5 and channel 7 do not follow a normal distribution, and it implies there may be a significant difference between the $\Delta BTHR$ and $\Delta ATHR$ in those channels. To find the most obvious difference between $\Delta BTHR$ and $\Delta ATHR$, the cosine similarity algorithm is adopted to find the smaller angle, which means more similarities between $\Delta BTHR$ and $\Delta ATHR$, and the result is shown in Table 3.

Table 3 The cosine similarity result in the AEB experiment

fNIRS channel	cosine similarity	degrees
channel 4	0.8648	30.1445
channel 5	0.9734	20.3859
channel 7	0.8325	33.6432

The average differences of the kinetic energy field and the cosine similarity degree of ΔTH in 2s between pre-stimulus and post-stimulus were calculated to quantify passengers' driving safety cognition, and the results are shown in illustration 26. The

average value of the cosine similarity degree of 14 samples is 39.2080° and the average difference value in the kinetic energy field is 2.2288, which ∗ indicates a cosine similarity degree, and ◊ indicates a kinetic energy field difference value.

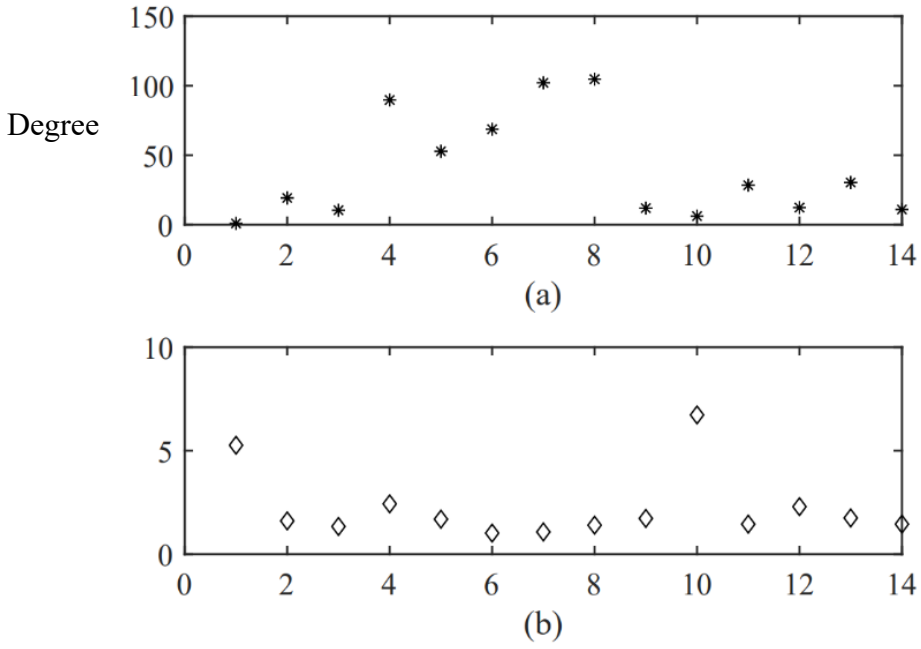

Illustration 26 AEB result: (a) Cosine similarity degree and (b) difference values of the kinetic energy field of channel 7

4.2.2 HWP Cut-in experiment results

The result of the Lilliefors test of the cut-in experiment is shown in Table 4.

Table 4 The distribution result of the data △BTHR and △ATHR in the HWP Cut-in experiment

channel / data	1	2	3	4	5	6	7	8
$\triangle ATHR$	0	0	0	0	0	0	1	0
$\triangle BTHR$	0	0	1	1	1	0	0	0

0 indicates data conform to normal distribution, and 1 otherwise.

It shows that the data of channels 1,2,6,8 follow a normal distribution. The values are shown in illustration 27, which shows the p value in channel 1 is the minimum.

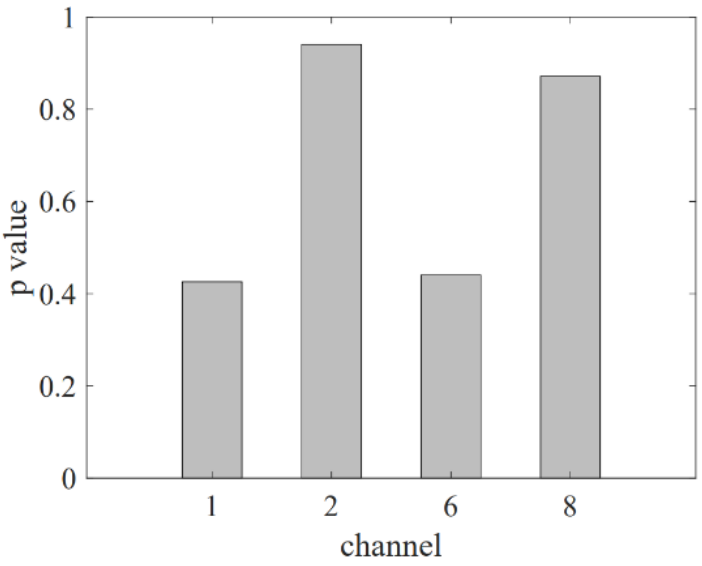

Illustration 27 The *p*-value for the HWP Cut-in test

The cosine similarity degree results of channel 1 and the channels in which the data $\Delta \mathrm{B}THR$ and $\Delta \mathrm{A}THR$ do not follow a normal distribution are shown in Table 5. From Table 5, we can find that the cosine similarity degree is maximum in channel 7 between $\Delta \mathrm{B}THR$ and $\Delta \mathrm{A}THR$ compared with other channels. The cosine similarity degree average value of those 9 samples is 13.0230° and the kinetic energy field average difference value is 0.3247, which $*$ indicates a cosine similarity degree, and $\diamond$ indicates a kinetic energy field difference value.

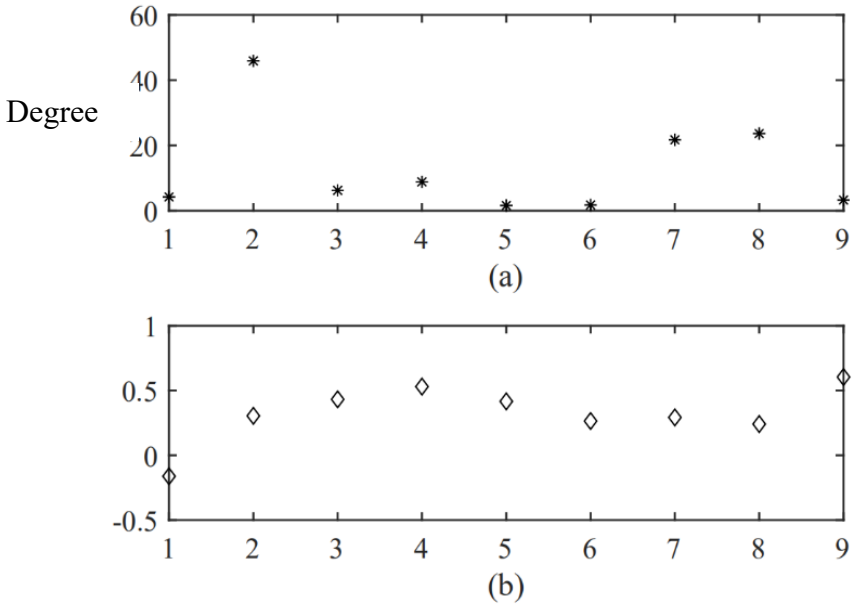

Illustration 28 HWP Cut-in result: (a) Cosine similarity degree and (b) difference values of the kinetic energy field of channel 7

Chapter 5: Conclusions and Future Work

5.1 EEG-Based Human-Centric Assistant Driving Systems

In this study, we first collected and analyzed the EEG signals of the passenger by ERP response analysis and found that different road events can be distinguished. The ERP features can be found at an average of 454 ms ± 234 ms before the actual button-pressing response. We also verified that the dorso-mesial part of the premotor cortex is related to brake intention or movement preparation [27]. Then we demonstrated that the proposed machine learning method was able to classify EEG signals of two street events with a high classification accuracy of 95.81%, which shows the probability of application on high-level autonomous vehicles. In the real-car experiment, passengers' reactions to emergency road events can be found at 310 ms before the AEB function of the vehicle was activated, which shows the potential of preventing accidents using the EEG signals of the passengers.

However, several limitations still existed in our study that can be improved in future research. First, the issue of lack of participants existed in this study and other several research [24], [25], [54]. For individual ERP response analysis, collecting data from more subjects can help reduce the noise and extract features. Although some studies have shown that age and gender effects are not critical, the relation between driving experience and response time had been proven that this could affect the performance of the BCI system related to the control of the autonomous vehicle [55]–[58].

There are other things that can be improved in the future. First, instead of finishing the experiment in one day. We designed the experiment with 4 2-hour sessions, which will notice if there are variations due to the different experiment period and subjects' status.

Although we asked them to come without any fatigue, this will help to eliminate the inconsistence. Moreover, we will design test runs for the subjects to make sure that they are familiar with the setup.

Our classification model for all subjects has a lower classification accuracy compared to the individual classification model. It is because of the unique brain anatomy of every person. Using customized EEG caps, or individual electrodes should be considered in the further data collection process. From the machine learning perspective, adding features such as subjects' information, and then selecting the best model for the different individuals can improve the performance of the classifier. Overall, detection system performance depends entirely on classifier performance and classifier performance is usually measured by classification accuracy [14]. The accuracy of the classifier is crucial to deploying the system on real vehicles. Even 99% accuracy is not enough because it is related to people's lives and public security. Moreover, since a car accident can happen fast, an online system with low latency is also required. All the classifiers are trained and tested on the computer with configurations that may improve the classification accuracy. However, a hardware-in-loop test is needed to verify if the configurations are realistic to deploy on a circuit board. For example, a filter with high orders performs better with higher latency.

In the real-car experiment, head movement due to emergency braking will affect the signal quality, which may lead to a problem for an online prediction model. Other issues such as portability of the EEG device, test duration to avoid fatigue effect, and the comparison of emergency and normal driving also need to be considered.

5.2 fNIRS passengers' driving risk cognition quantification

In this work, AEB and cut-in experiments were performed in the Dazu experimental base in China, and the cerebral oxygen exchange in the prefrontal cortex was obtained. A kinetic energy field was calculated based on ego vehicle and target vehicle information for indicating driving environment risk, and the point that the risk field change is maximum was selected as a stimulus moment. Then, we analyzed passengers' brain-sensitive region in the prefrontal cortex to risk change based on cerebral oxygen exchange data and the kinetic energy field difference between pre-stimulus and post-stimulus data in 2 seconds; finally, the results of AEB and cut-in experiments are compared, in two new points are found based those results in illustration 29, the one point is that compared with other channels, the channel 7 is sensitive to risk change; another point is that in a certain range, the risk field rises may bring about cerebral oxygen exchange increases. To further the brain-sensitive region to risk change in the Brodmann diagram, we check the position of channel 7 in the Brodmann diagram and find that channel 7 is located at BA 9.

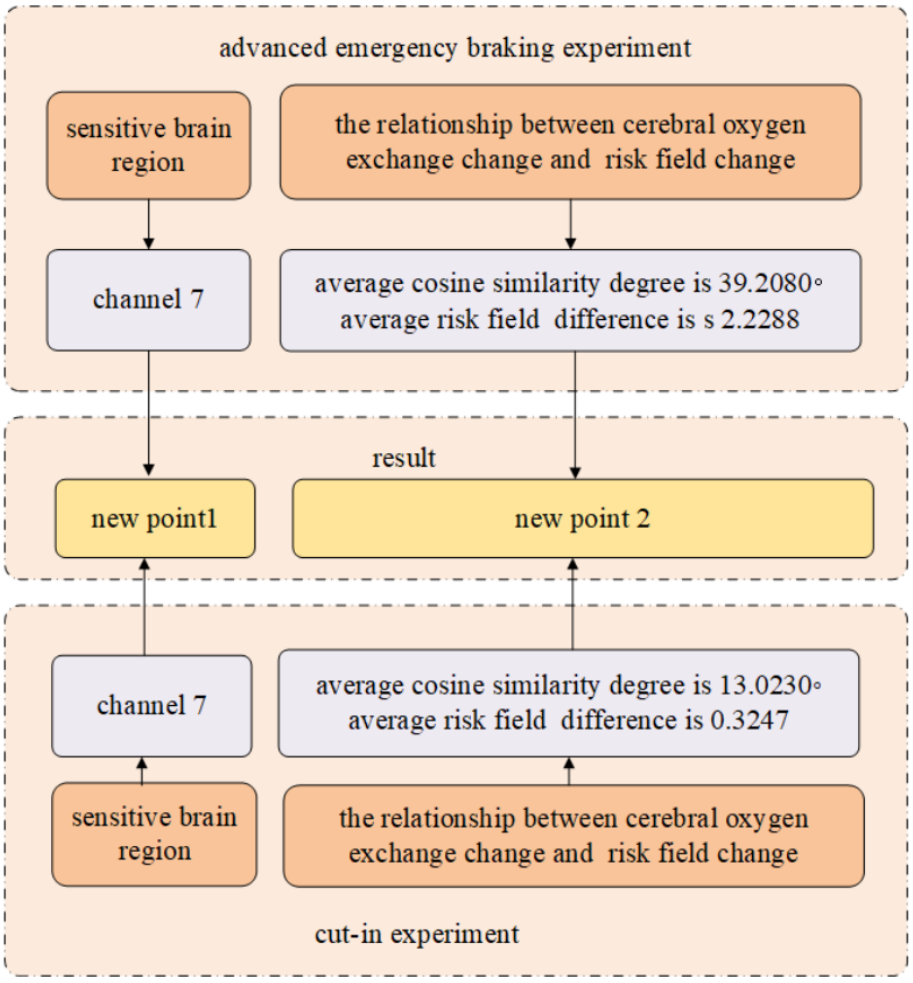

Illustration 29 Result flow chart

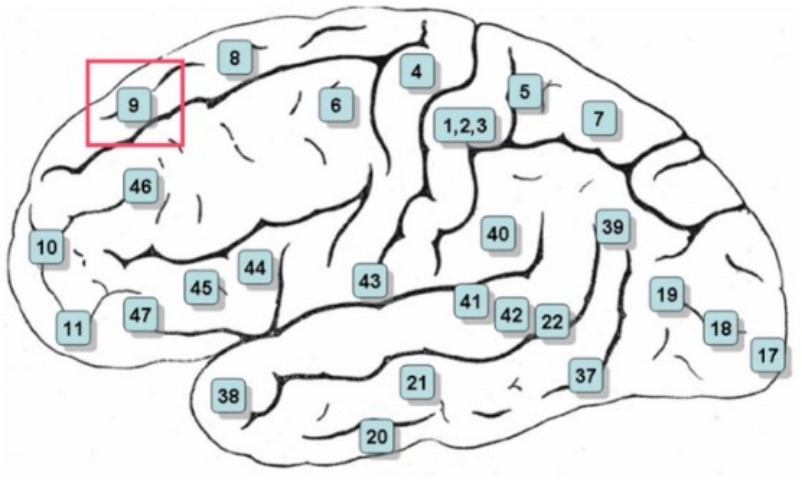

Illustration 30 Brodmann regions

5.3 Future Works

Future works of EEG study can be focused on different perspectives. First, in terms of decision system design, we need to clarify the operational design domain (ODD) of this system. In other words, the use case of systems involving EEG signals should be clarified to enhance driving safety and avoid false alarms. A system of brain-computer hybrid intelligence can be designed to prevent the safety concerns caused by misuse of the user or functional failure of autonomous vehicles. For the lack of the participant issue, we started our next stage experiments, which involved more than 20 participants with different age, sex, and driving experience. Moreover, a more robust system that is fused with other information such as other physiological signals, other sensor signals, road information, and other vehicles' information, can be designed. Finally, topics of machine ethics and driver's trust are also important for all high-level autonomous vehicles [59]–[61].

For fNIRS, we adopt a kinetic energy field to represent the driving environment risk degree, built a relationship between the kinetic energy field and the brain, and figured out the sensitive region to risk change in the prefrontal cortex of passengers. However, there are still some shortcomings in our research. The number of samples adopted in this experiment is relatively small, and the time window (2 seconds) was selected by experience. In the future, we will collect more data to analyze and explore the influence of the time window. Quantifying passengers' driving safety cognition is important for solving SOTIF problems, and it may help automated driving systems to prevent potentially dangerous behaviors caused by the expected function or performance limitation of systems.

Appendices

Appendix A Skilled Human Driver Performance Model

In UN Regulation No. 157 - Automated Lane Keeping Systems (ALKS), appendix 3 describes a human driver performance model and related parameters in the traffic critical disturbance scenarios, which can be useful to be compared those parameters with our findings. The illustration below shows the skilled human performance model from the simulation program. Since we do not require participants to press the brake pedal, the button-pressing action can be considered as pressing the brake pedal.

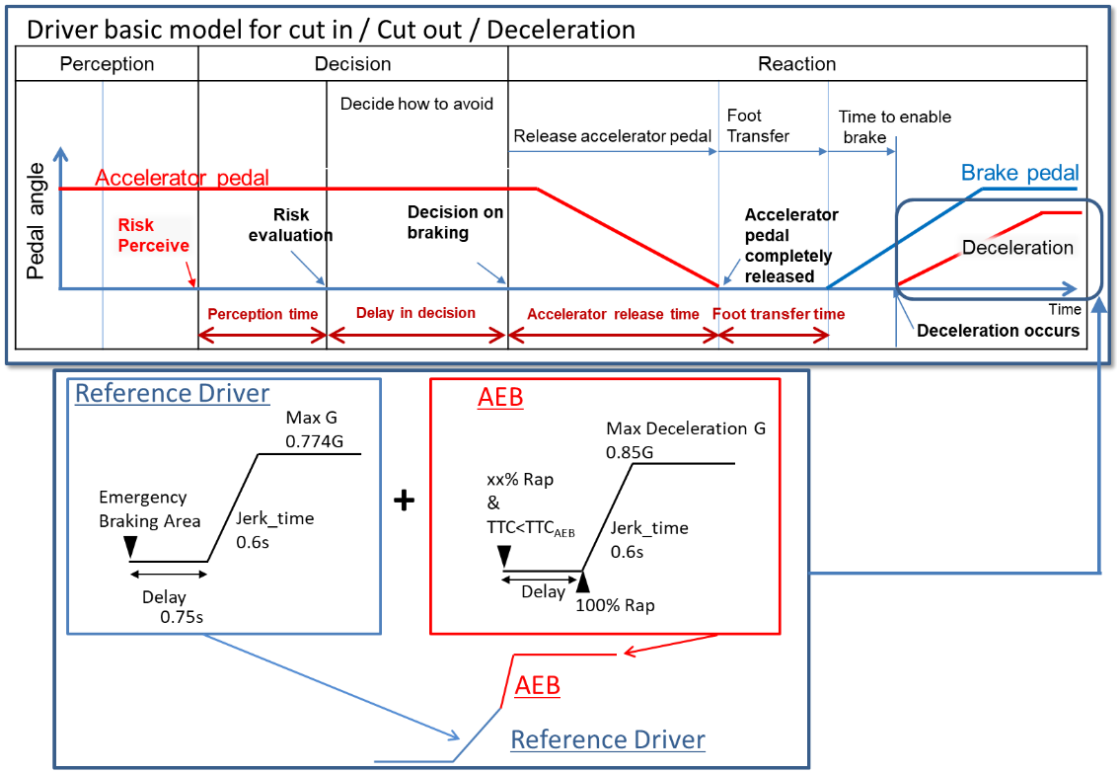

Illustration 31 Skilled human performance model [62]

The table below shows the performance model factors for vehicles. Two things that need to be mentioned are that the risk evaluation time is 0.4 s, which is similar to our finding

of 0.45 s. The sum of risk evaluation time and time duration from having finished perception until starting deceleration is 1.15 s, compared to our average reaction time of 1.384 s. The small difference is that our participants are not professional or skilled drivers.

Table 5 Performance model factors for vehicles

		Factors
Risk perception point	Lane change (cutting in, cutting out)	Deviation of the center of a vehicle over 0.375m from the center of the driving lane (derived from research by Japan)
	Deceleration	Deceleration ratio of the preceding vehicle and following distance of ego vehicle
Risk evaluation time		0.4 seconds (from research by Japan)
Time duration from having finished perception until starting deceleration		0.75 seconds (common data in Japan)
Jerking time to full deceleration (road friction 1.0)		0.6 seconds to 0.774G (from experiments by NHTSA and Japan)
Jerking time to full deceleration (after full wrap of ego vehicle and cut-in vehicle, road friction 1.0)		0.6 seconds to 0.85G (derived from UN Regulation No. 152 on AEBS)

Appendix B EEG Hardware Introduction

B.1 Hardware

EEG hardware used in this research is named TMSi SAGA 64+ from a Netherlands company. It can be used to collect physiological signals such as EEG and HD EMG, etc. There are two parts of the device: a data recorder and a docking station. The data recorder, shown in the illustration below, contains an amplifier that connects sensors for data acquisition. It can be powered by batteries or a docking station.

Illustration 32 TMSi Data Recorder

The docking station receives the raw physiological data from the data recorder and processes it before sending the data to the computer. To make sure that there is no delay during the data acquisition process, we did not use the processing function in the docking station and processed the raw data using MATLAB and EEGLAB.

Illustration 33 TMSi Docking Station

There are multiple ways for the data recorder and docking station to connect to each other, including a direct connection to the docking station, fiber optics, and WIFI. To ensure signal quality, we abandoned the WIFI method to avoid possible package loss during the data acquisition process. There are a couple of ways to connect the docking station to a PC: ethernet or USB cable. In addition to the wired/wireless method, TMSi provides saving data to an SD card.

Illustration 34 Direct connection to the docking station

In this research, we only used an EEG module to collect EEG signals, however, we can also combine a lead of EMG signal in future data collection, if we want to investigate drivers' foot movements. The EEG cap that is connected to the TMSi SAGA 64+ system is shown in the Illustration below.

Illustration 35 System with an EEG cap attached to

There are three types of EEG caps in terms of electrode types: gel headcap, water headcap, and dry headcap. Each type of headcap has its advantage. The water headcap uses water-based electrodes, which means it will shorten the preparation time, but the signal quality is the worst compared with the other two. For the dry headcap, the use of a dry electrode is perfect for capturing EEG signals while participants are moving or in an unstable environment. In this case, since the test vehicle will move and brake hard, it seems a better choice to collect EEG data in a real-car experiment. However, since there is no liquid/gel involved, the headcap needs to equip tight to avoid electrode shift, and it is not suitable for long-time data acquisition. Ag/AgCl electrode EEG cap is the most popular cap in EEG-related research. The only shortage of this headcap is that it needed a relatively long time for preparation (more than 45 mins).

Illustration 36 Dry EEG cap (Neuroelectrics) and water headcap (TMSi)

A conductive gel is used because we are using has Ag/AgCl electrode, which requires electrode gel to conduct between the scalp and electrodes. The conductive gel we used in the EEG experiment is Signagel® Electrode Gel from PARKER LABORATORIES, INC. in the US. It is a saline electrode gel, that can be used for multiple purposes such as EEG, EMG, and other physiological signal collection.

Illustration 37 PARKER Signagel® Electrode Gel

For the real-car experiment, we also used a digital trigger to track the participant's reaction as well as synchronize with the Controller Area Network (CAN bus). After the button is pressed, there will be a digital pulse that sends to both the EEG data recorder and the vehicle data capture system. After testing, we found the delay and time difference was less than 10 ms, which is acceptable for synchronization.

B.2 Software

TMSi provides software called TMSi Polybench with functions including real-time impedance check, real-time event marker, reference auto-switch, data filtering, processing, etc. We always check the impedance before and after every trial to make sure the EEG data is valid.

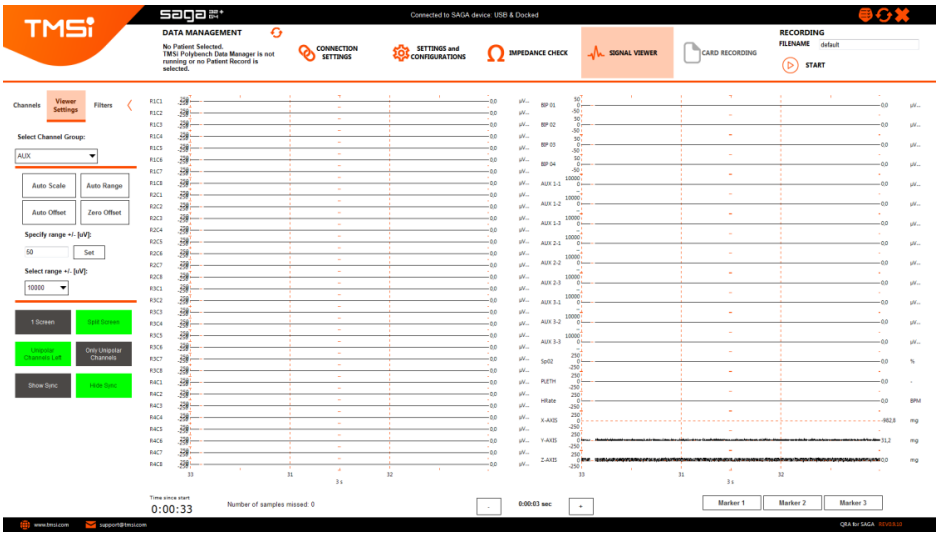

Illustration 38 TMSi Polybench

Appendix C Other participants' ERP Result

C.1 The pedestrian crossing events

In this section, the butterfly plot shows the important time we obtained in Table 1.

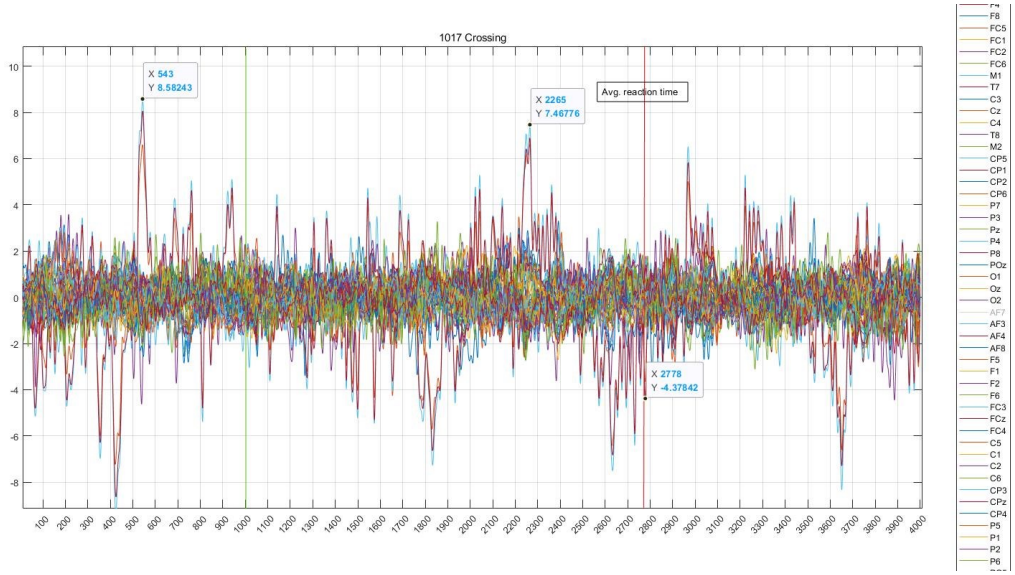

Illustration 39 Subject 1 ERP response for pedestrian crossing events

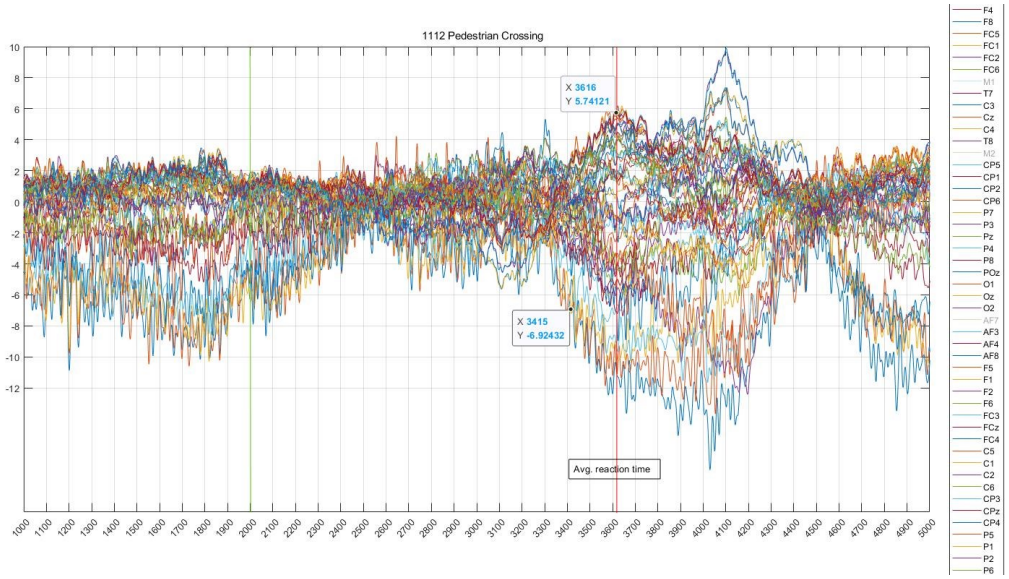

Illustration 40 Subject 2 ERP response for pedestrian crossing events

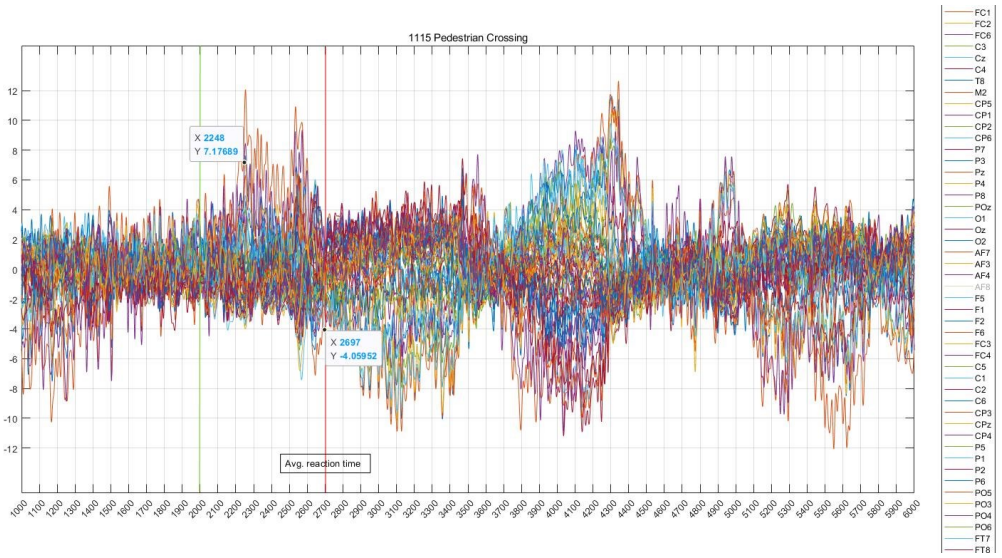

Illustration 41 Subject 3 ERP response for pedestrian crossing events

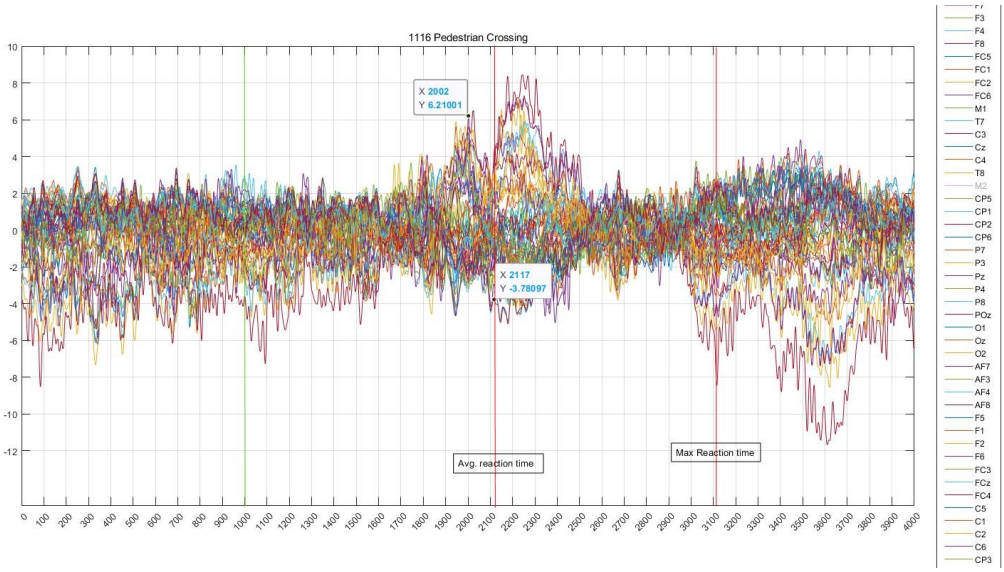

Illustration 42 Subject 4 ERP response for pedestrian crossing events

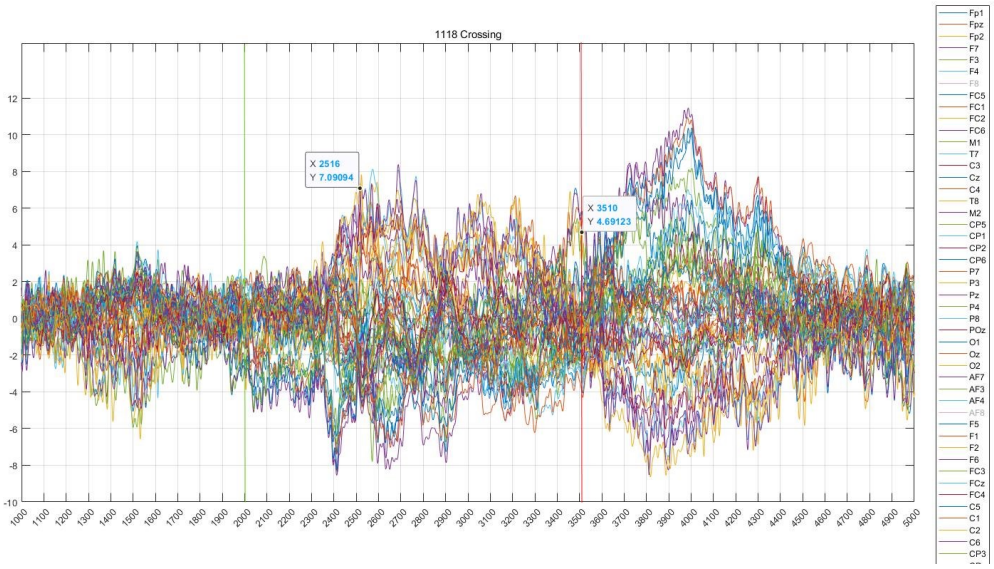

Illustration 43 Subject 5 ERP response for pedestrian crossing events

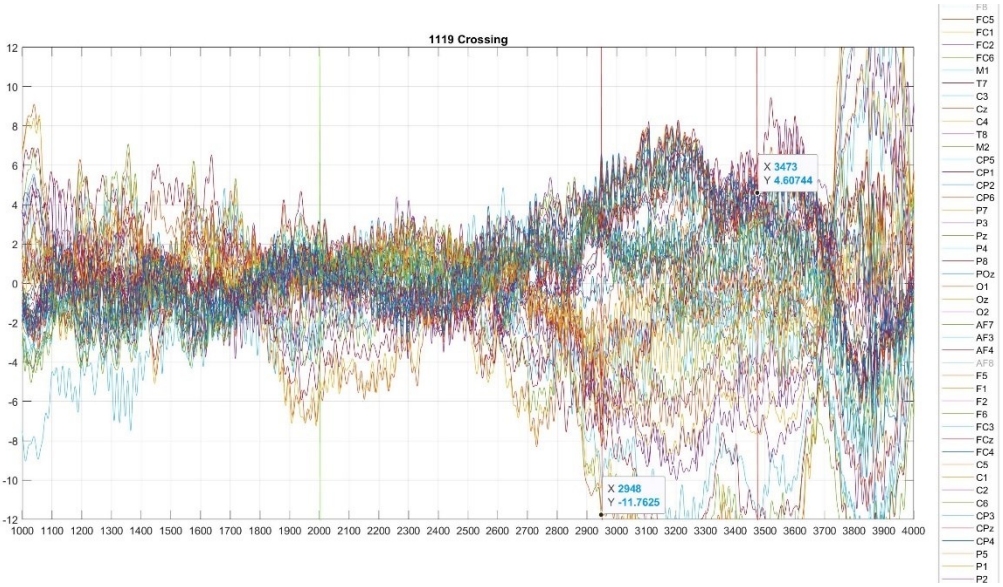

Illustration 44 Subject 6 ERP response for pedestrian crossing events

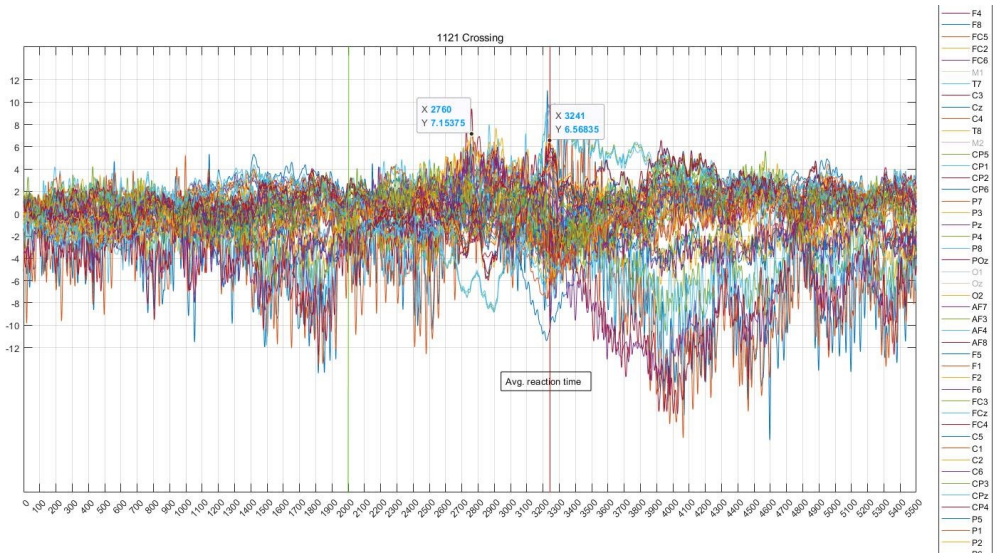

Illustration 45 Subject 7 ERP response for pedestrian crossing events

Illustration 46 Subject 8 ERP response for pedestrian crossing events

C.2 The pedestrian non-crossing events

We analyze the ERP response of participants watching a pedestrian stand on the curb. The results show that there is an ERP response caused by visual stimulus. However, the time a subject spotted a pedestrian is different. We could not obtain a common feature in the time domain for all subjects.

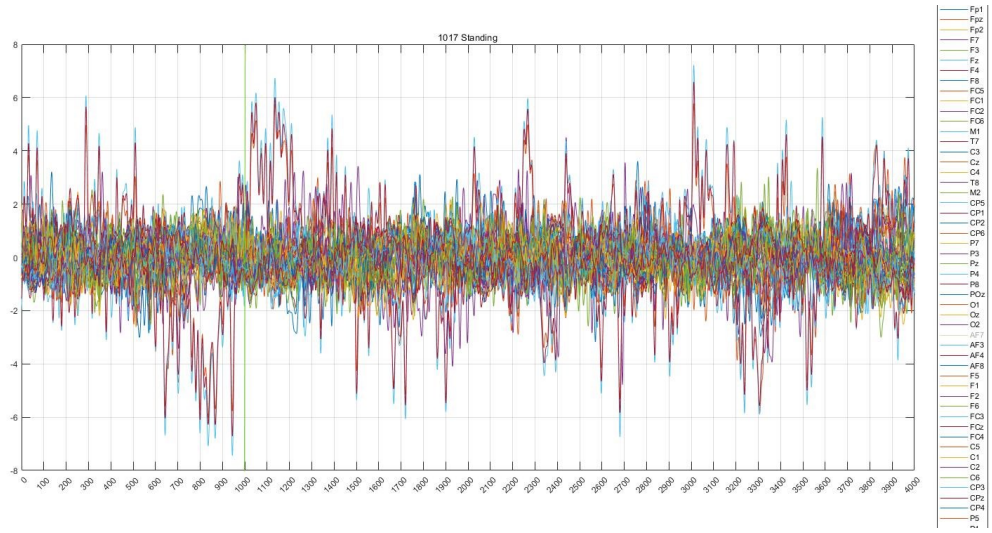

Illustration 47 Subject 1 ERP response for pedestrian non-crossing events

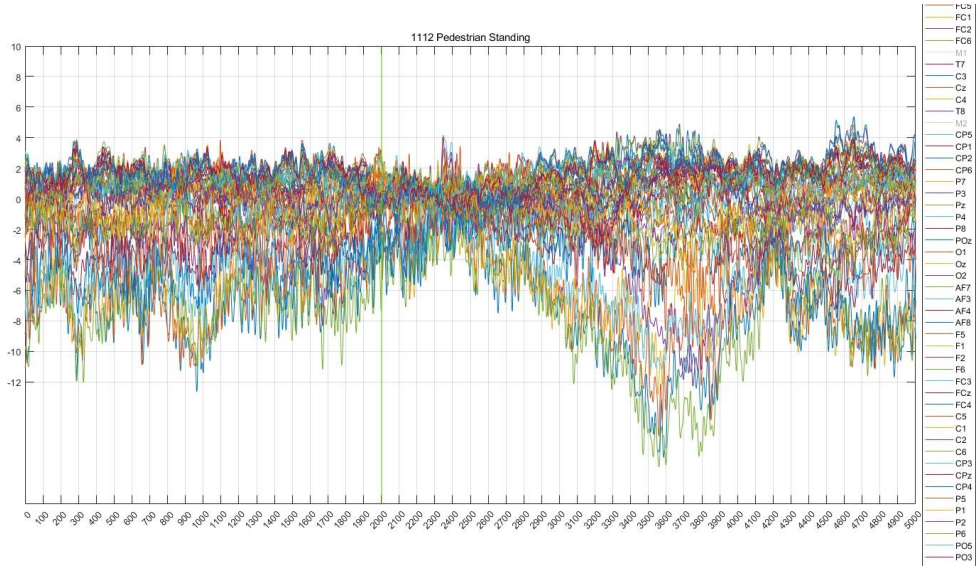

Illustration 48 Subject 2 ERP response for pedestrian non-crossing events

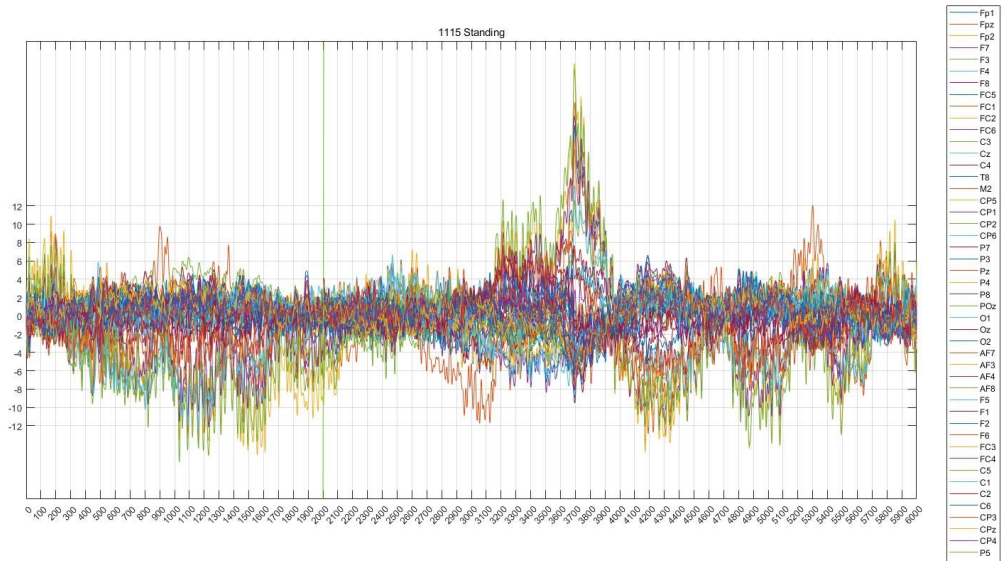

Illustration 49 Subject 3 ERP response for pedestrian non-crossing events

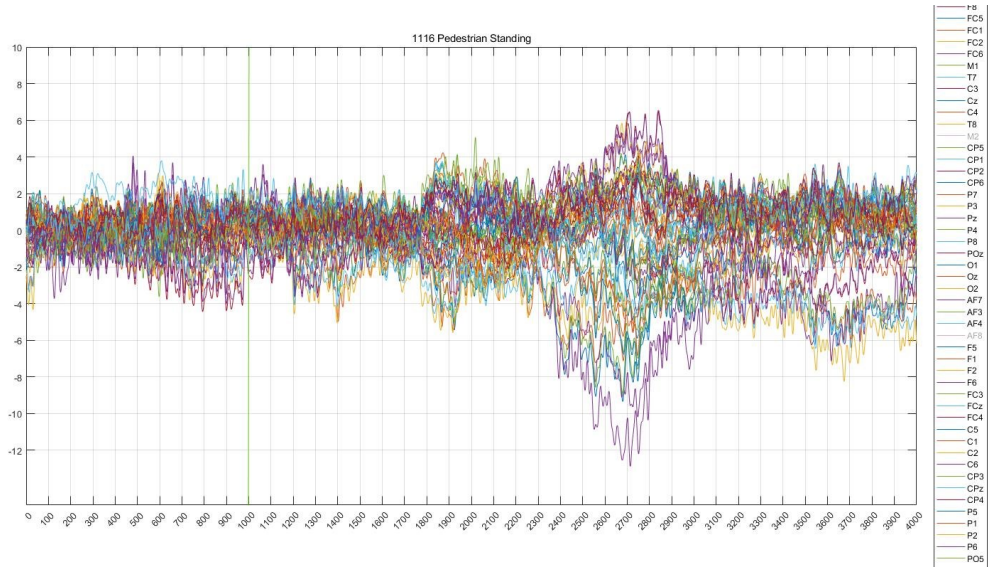

Illustration 50 Subject 4 ERP response for pedestrian non-crossing events

Illustration 51 Subject 5 ERP response for pedestrian non-crossing events

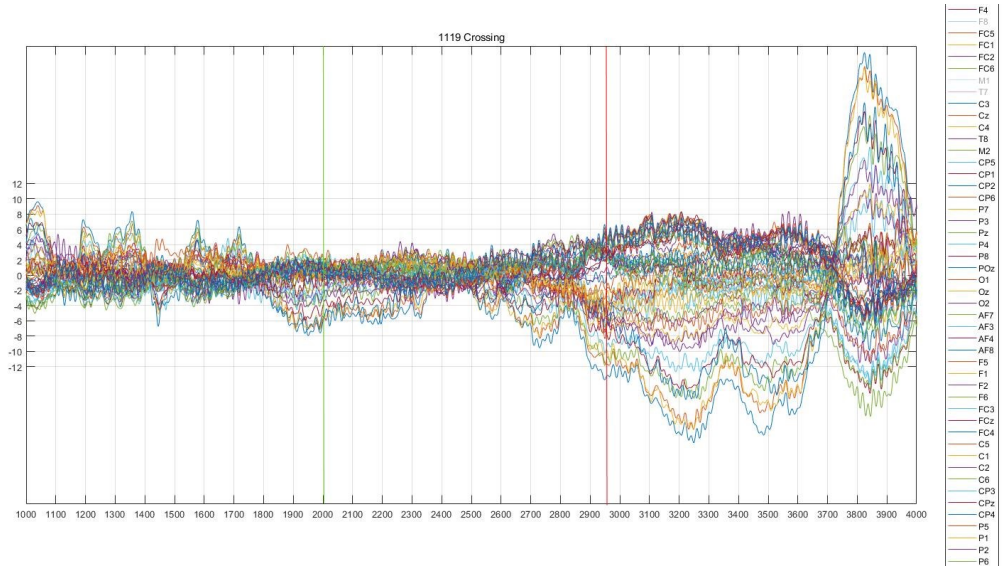

Illustration 52 Subject 6 ERP response for pedestrian non-crossing events

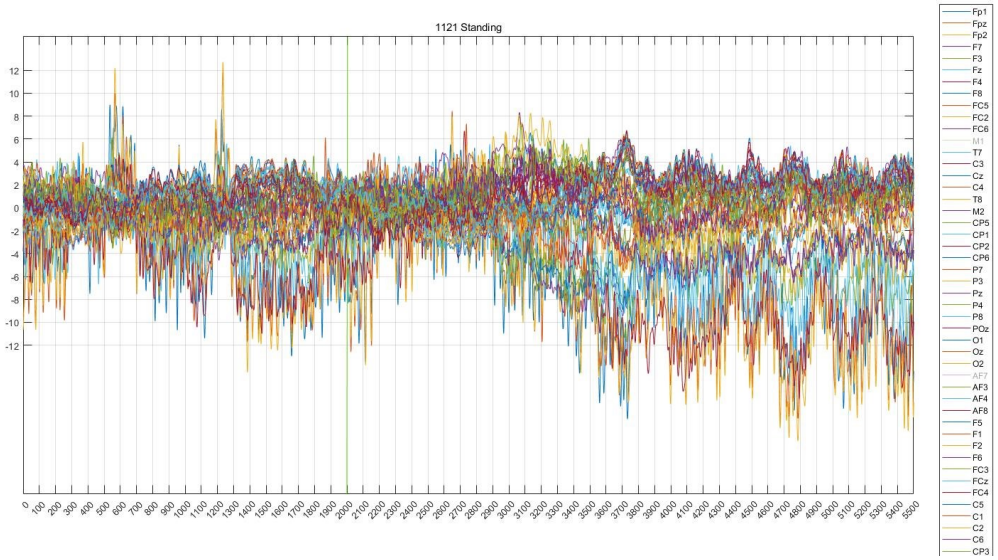

Illustration 53 Subject 7 ERP response for pedestrian non-crossing events

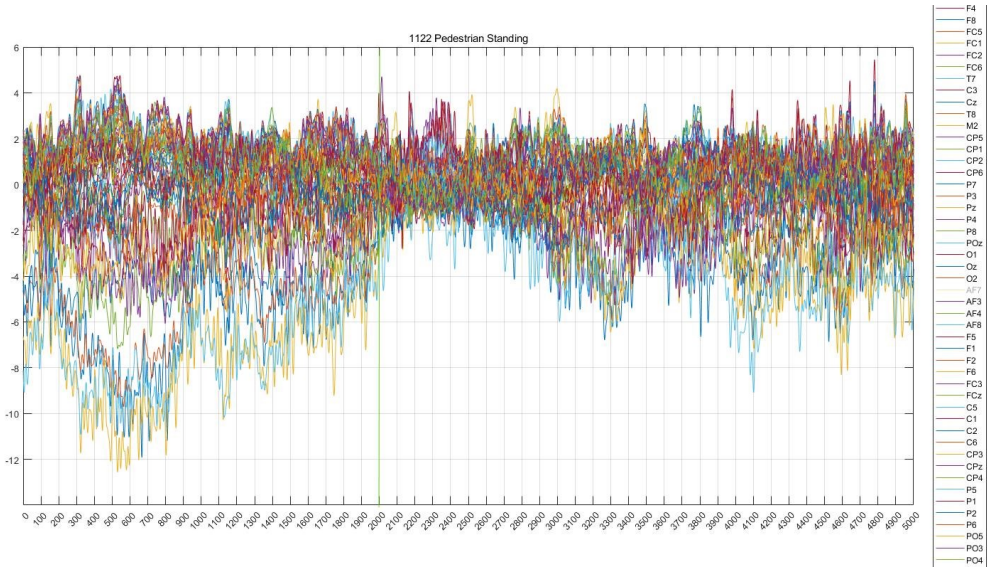

Illustration 54 Subject 8 ERP response for pedestrian non-crossing events

Bibliography

[1] J. Terken and B. Pfleging, “Toward Shared Control Between Automated Vehicles and Users,” *Automotive Innovation*, vol. 3, no. 1, 2020, doi: 10.1007/s42154-019-00087-9.

[2] M. Capallera *et al.*, “Owner manuals review and taxonomy of ADAS limitations in partially automated vehicles,” 2019. doi: 10.1145/3342197.3344530.

[3] International Organization for Standardization, “ISO 21448:2022 Road vehicles — Safety of the intended functionality,” *ISO/TC 22/SC 32 Electrical and electronic components and general system aspects*. International Organization for Standardization, pp. 1–10, Jun. 2022. Accessed: Sep. 01, 2022. [Online]. Available: https://www.iso.org/standard/77490.html

[4] Cadie Thompson, “New details about the fatal Tesla Autopilot crash reveal the driver’s last minutes,” *Insider*, Jun. 20, 2017.

[5] H. Wang, Y. Huang, A. Khajepour, Y. Zhang, Y. Rasekhipour, and D. Cao, “Crash Mitigation in Motion Planning for Autonomous Vehicles,” *IEEE Transactions on Intelligent Transportation Systems*, vol. 20, no. 9, 2019, doi: 10.1109/TITS.2018.2873921.

[6] Z. Wang, Y. Wu, and Q. Niu, “Multi-Sensor Fusion in Automated Driving: A Survey,” *IEEE Access*, vol. 8. 2020. doi: 10.1109/ACCESS.2019.2962554.

[7] Mark Venables, “Sensing an Autonomous Vehicle Future,” *The international society for optics and photonics*, Mar. 01, 2022.

[8] I. Rojas and F. Ortuño, “Bioinformatics and Biomedical Engineering.” [Online]. Available: http://www.springer.com/series/5381

[9] V. C. C. Roza and O. A. Postolache, “Multimodal approach for emotion recognition based on simulated flight experiments,” *Sensors (Switzerland)*, vol. 19, no. 24, Dec. 2019, doi: 10.3390/s19245516.

[10] M. E. Dawson, A. M. Schell, and D. L. Filion, “The electrodermal system,” in *Handbook of Psychophysiology, Fourth Edition*, Cambridge University Press, 2016, pp. 217–243. doi: 10.1017/9781107415782.010.

[11] A. Cruz, G. Pires, A. C. Lopes, and U. J. Nunes, *Detection of Stressful Situations Using GSR While Driving a BCI-controlled Wheelchair*. 2019. doi: 10.0/Linux-x86_64.

[12] S. Saha *et al.*, “Progress in Brain Computer Interface: Challenges and Opportunities,” *Frontiers in Systems Neuroscience*, vol. 15. 2021. doi: 10.3389/fnsys.2021.578875.

[13] L. F. Nicolas-Alonso and J. Gomez-Gil, “Brain computer interfaces, a review,” *Sensors*, vol. 12, no. 2. 2012. doi: 10.3390/s120201211.

[14] M. Rashid *et al.*, “Current Status, Challenges, and Possible Solutions of EEG-Based Brain-Computer Interface: A Comprehensive Review,” *Frontiers in Neurorobotics*, vol. 14. Frontiers Media S.A., Jun. 03, 2020. doi: 10.3389/fnbot.2020.00025.

[15] H. Aghajani, M. Garbey, and A. Omurtag, “Measuring mental workload with EEG+fNIRS,” *Front Hum Neurosci*, vol. 11, Jul. 2017, doi: 10.3389/fnhum.2017.00359.

[16] Y. Chen *et al.*, "Amplitude of fNIRS Resting-State Global Signal Is Related to EEG Vigilance Measures: A Simultaneous fNIRS and EEG Study," *Front Neurosci*, vol. 14, 2020, doi: 10.3389/fnins.2020.560878.

[17] J. Uchitel, E. E. Vidal-Rosas, R. J. Cooper, and H. Zhao, "Wearable, integrated eeg–fnirs technologies: A review," *Sensors*, vol. 21, no. 18. 2021. doi: 10.3390/s21186106.

[18] Y. Sun, H. Ayaz, and A. N. Akansu, "Multimodal affective state assessment using fNIRS+ EEG and spontaneous facial expression," *Brain Sci*, vol. 10, no. 2, 2020, doi: 10.3390/brainsci10020085.

[19] J. Minguillon, E. Perez, M. A. Lopez-Gordo, F. Pelayo, and M. J. Sanchez-Carrion, "Portable system for real-time detection of stress level," *Sensors (Switzerland)*, vol. 18, no. 8, 2018, doi: 10.3390/s18082504.

[20] G. Rigas, Y. Goletsis, and D. I. Fotiadis, "Real-time driver's stress event detection," *IEEE Transactions on Intelligent Transportation Systems*, vol. 13, no. 1, pp. 221–234, Mar. 2012, doi: 10.1109/TITS.2011.2168215.

[21] K. Wang, Y. L. Murphey, Y. Zhou, X. Hu, and X. Zhang, "Detection of driver stress in real-world driving environment using physiological signals," 2019.

[22] P. D. Purnamasari and A. Fernandya, "Real time EEG-based stress detection and meditation application with K-nearest neighbor," in *IEEE Region 10 Humanitarian Technology Conference, R10-HTC*, Nov. 2019, vol. 2019-November. doi: 10.1109/R10-HTC47129.2019.9042488.

[23] I. H. Kim, J. W. Kim, S. Haufe, and S. W. Lee, “Detection of braking intention in diverse situations during simulated driving based on EEG feature combination,” *J Neural Eng*, vol. 12, no. 1, Feb. 2015, doi: 10.1088/1741-2560/12/1/016001.

[24] S. Haufe, M. S. Treder, M. F. Gugler, M. Sagebaum, G. Curio, and B. Blankertz, “EEG potentials predict upcoming emergency brakings during simulated driving,” *J Neural Eng*, vol. 8, no. 5, Oct. 2011, doi: 10.1088/1741-2560/8/5/056001.

[25] L. Bi, H. Wang, T. Teng, and C. Guan, “A Novel Method of Emergency Situation Detection for a Brain-Controlled Vehicle by Combining EEG Signals with Surrounding Information,” *IEEE Transactions on Neural Systems and Rehabilitation Engineering*, vol. 26, no. 10, pp. 1926–1934, Oct. 2018, doi: 10.1109/TNSRE.2018.2868486.

[26] Y. Lu and L. Bi, “Combined Lateral and Longitudinal Control of EEG Signals-Based Brain-Controlled Vehicles,” *IEEE Trans Neural Syst Rehabil Eng*, vol. 27, no. 9, 2019, doi: 10.1109/TNSRE.2019.2931360.

[27] G. Vecchiato *et al.*, “Electroencephalographic time-frequency patterns of braking and acceleration movement preparation in car driving simulation,” *Brain Res*, vol. 1716, pp. 16–26, Aug. 2019, doi: 10.1016/j.brainres.2018.09.004.

[28] Z. Khaliliardali, R. Chavarriaga, L. A. Gheorghe, and J. D. R. Millán, “Action prediction based on anticipatory brain potentials during simulated driving,” *J Neural Eng*, vol. 12, no. 6, 2015, doi: 10.1088/1741-2560/12/6/066006.

[29] D. Gérard, M. Kévin, D. Gérard, T. E. Ward, and P. Stéphane, “NIRS-measured prefrontal cortex activity in neuroergonomics: strengths and weaknesses,” *Front Hum Neurosci*, vol. 7, p. 583, 2013.

[30] A. R. Harrivel, D. H. Weissman, D. C. Noll, and S. J. Peltier, "Monitoring attentional state with fNIRS," *Front Hum Neurosci*, vol. 7, p. 861, 2013.

[31] W. J. Horrey, M. F. Lesch, A. Garabet, L. Simmons, and R. Maikala, "Distraction and task engagement: How interesting and boring information impact driving performance and subjective and physiological responses," *Appl Ergon*, vol. 58, pp. 342–348, 2017.

[32] S. Balters, S. Sibi, M. Johns, M. Steinert, and W. Ju, "Learning-by-doing: using near infrared spectroscopy to detect habituation and adaptation in automated driving," in *Proceedings of the 9th International Conference on Automotive User Interfaces and Interactive Vehicular Applications*, 2017, pp. 134–143.

[33] Y. Orino *et al.*, "Relationship between brain activity and real-road driving behavior: a vector-based whole-brain functional near-infrared spectroscopy study," in *Driving Assessment Conference*, 2017, pp. 16–22.

[34] L. Xu, B. Wang, G. Xu, W. Wang, Z. Liu, and Z. Li, "Functional connectivity analysis using fNIRS in healthy subjects during prolonged simulated driving," *Neurosci Lett*, vol. 640, pp. 21–28, 2017.

[35] J. L. Bruno *et al.*, "Mind over motor mapping: Driver response to changing vehicle dynamics," *Hum Brain Mapp*, vol. 39, no. 10, pp. 3915–3927, 2018.

[36] A. S. Le, H. Aoki, F. Murase, and K. Ishida, "A novel method for classifying driver mental workload under naturalistic conditions with information from near-infrared spectroscopy," *Front Hum Neurosci*, p. 431, 2018.

[37] A. R. Hidalgo-Muñoz *et al.*, "Hemodynamic responses to visual cues during attentive listening in autonomous versus manual simulated driving: A pilot study," *Brain Cogn*, vol. 135, p. 103583, 2019.

[38] C. F. Geissler, J. Schneider, and C. Frings, "Shedding light on the prefrontal correlates of mental workload in simulated driving: a functional near-infrared spectroscopy study," *Sci Rep*, vol. 11, no. 1, pp. 1–10, 2021.

[39] L. Zhu *et al.*, "Analysis of braking intention based on fNIRS in driving simulation experiments," *IET Intelligent Transport Systems*, vol. 13, no. 7, pp. 1181–1189, 2019.

[40] G. Huve, K. Takahashi, and M. Hashimoto, "Online recognition of the mental states of drivers with an fnirs-based brain-computer interface using deep neural network," in *2019 IEEE International Conference on Mechatronics (ICM)*, 2019, vol. 1, pp. 238–242.

[41] NHS, "Electroencephalogram (EEG)," *NHS*, Jan. 05, 2022.

[42] S. J. Luck, "An Introduction to the Event-Related Potential Technique."

[43] A. Delorme and S. Makeig, "EEGLAB: An open source toolbox for analysis of single-trial EEG dynamics including independent component analysis," *J Neurosci Methods*, vol. 134, no. 1, 2004, doi: 10.1016/j.jneumeth.2003.10.009.

[44] Z. J. Koles, "The quantitative extraction and topographic mapping of the abnormal components in the clinical EEG," *Electroencephalogr Clin Neurophysiol*, vol. 79, no. 6, 1991, doi: 10.1016/0013-4694(91)90163-X.

[45] Christian A. Kothe, “Introduction to Modern Brain-Computer Interface Design,” 2013. Accessed: Sep. 01, 2022. [Online]. Available: ftp://sccn.ucsd.edu/pub/bcilab/lectures/07_Oscillatory_Processes.pdf

[46] E. Neto, F. Biessmann, H. Aurlien, H. Nordby, and T. Eichele, “Regularized linear discriminant analysis of EEG features in dementia patients,” *Front Aging Neurosci*, vol. 8, no. NOV, 2016, doi: 10.3389/fnagi.2016.00273.

[47] F. Pedregosa *et al.*, “Scikit-learn: Machine learning in Python,” *Journal of Machine Learning Research*, vol. 12, 2011.

[48] M. Cope, “THE APPLICATION OF NEAR INFRARED SPECTROSCOPY TO NON INVASIVE MONITORING OF CEREBRAL OXYGENATION IN THE NEWBORN INFANT,” 1991.

[49] P. Pinti *et al.*, “The present and future use of functional near-infrared spectroscopy (fNIRS) for cognitive neuroscience,” *Ann N Y Acad Sci*, vol. 1464, no. 1, pp. 5–29, 2020.

[50] W. Jianqiang, W. Jian, and L. I. Yang, “Concept, principle and modeling of driving risk field based on driver-vehicle-road interaction,” *China Journal of Highway and Transport*, vol. 29, no. 1, p. 105, 2016.

[51] T. Kato, “Principle and technique of NIRS-Imaging for human brain FORCE: fast-oxygen response in capillary event,” in *International Congress Series*, 2004, vol. 1270, pp. 85–90.

[52] M. Sano, S. Sano, N. Oka, K. Yoshino, and T. Kato, “Increased oxygen load in the prefrontal cortex from mouth breathing: a vector-based near-infrared spectroscopy study,” *Neuroreport*, vol. 24, no. 17, p. 935, 2013.

[53] Z. Chenyang, L. I. Shuguang, L. I. Yaohua, Y. A. O. Jin, Z. H. U. Lei, and W. Min, "Differences of the motion sickness associated brain activity regions based on the driving simulator and fNIRS," *Journal of Automotive Safety and Energy*, vol. 10, no. 4, p. 433, 2019.

[54] T. H. Nguyen and W. Y. Chung, "Detection of driver braking intention using EEG signals during simulated driving," *Sensors (Switzerland)*, vol. 19, no. 13, 2019, doi: 10.3390/s19132863.

[55] C. Guger *et al.*, "How many people could use an SSVEP BCI?," *Front Neurosci*, no. NOV, 2012, doi: 10.3389/fnins.2012.00169.

[56] C. Guger *et al.*, "How many people are able to control a P300-based brain-computer interface (BCI)?," *Neurosci Lett*, vol. 462, no. 1, 2009, doi: 10.1016/j.neulet.2009.06.045.

[57] B. Allison, T. Lüth, D. Valbuena, A. Teymourian, I. Volosyak, and A. Gräser, "BCI demographics: How many (and what kinds of) people can use an SSVEP BCI?," *IEEE Transactions on Neural Systems and Rehabilitation Engineering*, vol. 18, no. 2, 2010, doi: 10.1109/TNSRE.2009.2039495.

[58] I. Volosyak, D. Valbuena, T. Lüth, T. Malechka, and A. Gräser, "BCI demographics II: How many (and What Kinds of) people can use a high-frequency SSVEP BCI?," *IEEE Transactions on Neural Systems and Rehabilitation Engineering*, vol. 19, no. 3, 2011, doi: 10.1109/TNSRE.2011.2121919.

[59] H. Wang, A. Khajepour, D. Cao, and T. Liu, "Ethical Decision Making in Autonomous Vehicles: Challenges and Research Progress," *IEEE Intelligent*

Transportation Systems Magazine, vol. 14, no. 1, 2022, doi: 10.1109/MITS.2019.2953556.

[60] H. Wang, Y. Huang, A. Khajepour, D. Cao, and C. Lv, "Ethical Decision-Making Platform in Autonomous Vehicles with Lexicographic Optimization Based Model Predictive Controller," *IEEE Trans Veh Technol*, vol. 69, no. 8, 2020, doi: 10.1109/TVT.2020.2996954.

[61] W. Li *et al.*, "Personality Openness Predicts Driver Trust in Automated Driving," *Automotive Innovation*, vol. 3, no. 1, 2020, doi: 10.1007/s42154-019-00086-w.

[62] UNITED NATIONS, "UN Regulation No. 157 - Automated Lane Keeping Systems (ALKS)," Mar. 2021. Accessed: Sep. 01, 2022. [Online]. Available: https://unece.org/transport/documents/2021/03/standards/un-regulation-no-157-automated-lane-keeping-systems-alks